Reentrant Phenomena in Relaxors

Chapter · March 2016

DOI: 10.1002/9781118935743.ch23

2 authors:

Alexei A Bokov
Simon Fraser University
163 PUBLICATIONS **7,409** CITATIONS
SEE PROFILE

Zuo-Guang Ye
Simon Fraser University
611 PUBLICATIONS **20,871** CITATIONS
SEE PROFILE

23

Reentrant Phenomena in Relaxors

Alexei A. Bokov and Zuo-Guang Ye

Department of Chemistry and 4D LABS, Simon Fraser University, Canada

23.1 Introduction

The sequence of phases observed in a material in the course of decreasing temperature typically obeys the general rule: a disordered (high-symmetry) phase is followed by a more ordered one. Normally the transition between phases is sharp, i.e. the order parameter, which is zero in the disordered phase, emerges at the transition temperature, T_C, when entering the ordered phase. While the regions of order parameter (fluctuations) may be observed locally at $T > T_C$, they are not stable and, therefore, short-lived. The classical examples of such a kind of behavior are ferromagnetic (FM) and ferroelectric (FE) phase transitions, where the order parameter is magnetization and electric polarization, respectively. However, in some instances this simple picture does not hold. The first example is relaxor ferroelectrics (or relaxors in short) where, between a high-temperature paraelectric (disordered) phase and a low-temperature ferroelectric (ordered) phase, one can observe a so-called ergodic relaxor (ER) phase in a rather wide temperature interval (dozens or even hundreds of degrees). Macroscopically the ER state possesses the same (high) symmetry as the paraelectric phase, but on the nanometer scale it contains areas of randomly oriented local polarization usually called polar nanoregions (PNRs). In contrast to FE fluctuations, PNRs are permanent, but the direction and magnitude of their dipole moments may fluctuate in time, giving rise to the extraordinary properties of relaxors, such as a giant dielectric constant, high electrostriction, characteristic dielectric dispersion, etc.

In a number of relaxor ferroelectrics (sometimes called "canonical" relaxors) the ER phase does not undergo the transition to the FE phase in a zero-field cooling regime and

Nanoscale Ferroelectrics and Multiferroics: Key Processing and Characterization Issues, and Nanoscale Effects, First Edition. Edited by Miguel Algueró, J. Marty Gregg, and Liliana Mitoseriu.

the macroscopic symmetry of the paraelectric phase remains unchanged down to near-zero K. In this case a thermodynamic transition from the ER state to a non-ergodic relaxor (NR) phase can be observed around the freezing temperature, below which the temporal fluctuations of PNRs vanish and their local polarization becomes static. The main microscopic reason for the freezing in canonical ferroelectric relaxors is believed to be the frustrated electric (and probably elastic) interactions among the dipoles of PNRs, which is similar to the one for the freezing in magnetic spin glasses, where the interactions occur among the diluted magnetic spins. Accordingly, many features of relaxor ferroelectrics and spin glasses are similar.

Another kind of unusual phase sequence is also known in which, after having gone through the disordered and the ordered phases, the material reenters a disordered phase upon further cooling. The low-temperature phase is called a reentrant or reappearing phase. It is not exactly the same as the high-temperature parent phase, but it loses the order parameter inherent in the intermediate (ordered) phase. This can happen if the entropy of the reentrant disordered phase is smaller than that of the ordered phase, and it implies that the considered order parameter does not reflect fully the order–disorder processes in the system. Besides the true reentrant behavior, situations are also possible where the order parameter of the intermediate phase is conserved in the low-temperature phase, but the macroscopic properties of the latter resemble the properties of a disordered phase. This can happen if some additional degrees of freedom not influencing the primary order parameter are involved in the reentrant transition. For example, in some magnets undergoing a paramagnetic–ferromagnetic–spin-glass sequence of phases, the primary order parameter (magnetization) increases monotonically from the Curie temperature down to near-zero K, but the spin-glass order appears at the reentrant transition in the direction perpendicular to the magnetization, leading to the coexistence of ferromagnetic and spin-glass orders. Such a kind of quasi-reentrant phase and true reentrant phase are often hardly distinguishable in experiments. Therefore, they are all commonly called reentrant phases.

The present chapter provides a comprehensive review on the reentrant relaxors, that is the materials in which both types of above-mentioned peculiarities (reentrant and relaxor behaviors) are observed.

23.2 Reentrant Phases in Condensed Matter

The first example of a reentrant phase transition was predicted theoretically more than a century ago by G. Tamman (1903) [1]. He considered a pressure–temperature phase diagram containing closed loops with a crystalline phase surrounded by liquid or glass regions, which implied reversible transition from the crystalline to an amorphous phase on cooling. This transition was termed inverse melting. It was initially believed that inverse melting could be seen only under extreme conditions inaccessible in a laboratory, but this phenomenon has since been observed at moderate temperatures and pressures in some polymers [2, 3].

Experimentally the reentrance was first discovered in binary liquid mixtures [4, 5]. It was found that certain homogeneous liquids transform into two separated, coexisting liquid phases at lower temperatures and become homogeneous again when the temperature is further lowered. The reentrant phenomena were studied elaborately in dilute magnets,

where the sequence of phases from paramagnetic to ferro- (or antiferro-)magnetic and further to reentrant spin glass (SG) was observed within a particular (usually narrow) concentration range of magnetic atoms. Other examples are superconductors with normal-superconducting-normal phase sequence [6–8] and liquid crystals in which multiple reentrance can be observed when nematic (less ordered) and smectic (more ordered) phases alternate several times as the temperature decreases [9, 10]. Recently a new astrophysical phenomenon of reentrant phase transition has been reported in which a monotonic variation of the temperature yields two phase transitions from large to small, and back to large, black holes [11]. Among ferroelectric crystals reentrant phases are comparatively seldom. Interestingly, however, the reentrant behavior was observed in the first known ferroelectric, Rochelle salt, which exhibits an FE phase between two Curie points (at 24 and –18 °C), that is between two paraelectric phases. KNO_3 and some complex organic compounds also exhibit similar behavior with two Curie points [12].

The equilibrium sequence of phases is determined by thermodynamics, which requires that the stable state of a matter should have a minimal free energy $F = U - ST$. At low temperatures the minimum of F corresponds to the minimum of internal energy, U. The internal energy is determined by the configuration of chemical bonds which are more or less symmetric. At high temperatures the second (negative) term in the free energy expression can prevail, giving rise to a state with large entropy (S), that is a disordered state. The change from the disordered to the ordered state is observed at the phase transition temperature, where the increase of $-TS$ due to ordering is compensated by the decrease of U. However, at lower temperatures where the reentrant transition occurs, the decrease of $-TS$ related to the vanishing of the order parameter leads to a much smaller change of F than the corresponding increase of U. Therefore, some hidden mechanism should exist that keeps the energy low. For example, in binary fluid mixtures, due to the interplay between the van der Waals and hydrogen bonds, a small increase of compositional (related to the order parameter) entropy upon transition to the reentrant phase is accompanied by a more significant decrease of orientational entropy and, as a result, the total entropy actually decreases [13].

To discuss the reentrant behavior in detail we will use as an example the magnetic reentrant spin glasses that are apparently the closest well-studied analogue to the poorly understood reentrant relaxors. Among the magnetic materials the reentrant behavior is typically observed in solid solutions where a "normal" spin-glass phase also exists, but in a different concentration range. Spin-glass phases appear when an FM or AFM system is diluted with magnetic or non-magnetic atoms and the interactions among spins become frustrated, that is a competition between the FM and AFM exchanges develops. A typical phase diagram of such a system is shown in Figure 23.1. As long as the dopant concentration (x) remains small, the original (FM or AFM) exchange dominates and the long-range ordered phase survives, though the transition temperature decreases with increasing x. The degree of frustration increases as well, and above the critical concentration, x_c, the competing FM and AFM interactions become balanced to destroy completely the long-range collinearity among the spins. As a result, the system transforms from the paramagnetic to the spin-glass (SG) phase as the temperature is decreased. However, in a comparatively narrow concentration interval below x_c, where the exchange interactions are frustrated only partially, two phase transitions can be observed. The first one is the Curie (or Néel) point and the second one is a transition to the phase with the properties characteristic of the SG phase, which is usually referred to as reentrant spin glass (RSG). This behavior has been found in

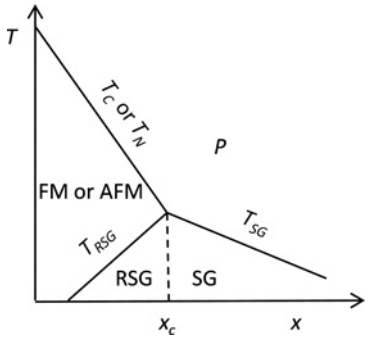

Figure 23.1 *Typical phase diagram of a reentrant spin-glass magnetic system showing paramagnetic (P), ferromagnetic (FM), or antiferromagnetic (AFM), spin-glass (SG) and reentrant spin-glass (RSG) phases; x is the concentration of non-magnetic atoms*

many materials, including polycrystalline metals Au_xFe_{1-x} [14] and $Ni_{1-x}Mn_x$ [15], dilute magnetic semiconductors $Eu_xSr_{1-x}S$ [16], amorphous metals $(Fe_{1-x}Mn_x)_{75}P_{16}B_6Al_3$ [17], etc. Figure 23.2 shows an example of RSG behavior in antiferromagnetic $Fe_{0.55}Mg_{0.45}Cl_2$. The maximum at 8 K in the temperature dependence of the real part of AC susceptibility is associated with the transition from the high-temperature paramagnetic phase to the AFM phase, while the anomaly with a significant dispersion in the frequency range of ~10 Hz–3 kHz observed at ~3 K indicates the transformation to the RSG phase. Magnetic relaxation at such low frequencies is typically absent in FM or AFM phases, but is characteristic of spin glasses.

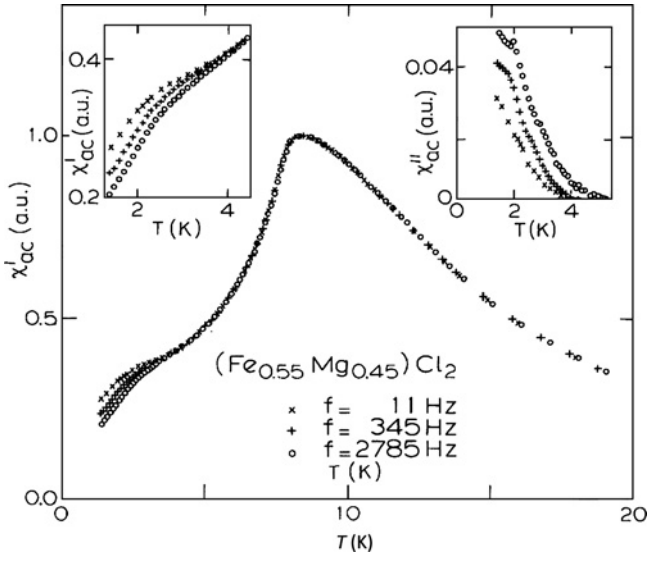

Figure 23.2 *Temperature dependence of the complex ac magnetic susceptibility ($\chi'_{ac} - i\chi''_{ac}$) of the dilute Ising antiferromagnet $Fe_{0.55}Mg_{0.45}Cl_2$ measured parallel to the easy axis at three different frequencies. Reprinted (Figure 2) from [18] with permission from Wong et al. Copyright (1985), American Physical Society*

While numerous experiments demonstrate that the macroscopic properties of RSG and usual SG phases are basically similar, the relations between their magnetic structures and microscopic mechanisms have been topics of intensive debates [19,20]. The phase diagram as depicted in Figure 23.1 was first derived theoretically in the classical work of Sherrington and Kirkpatrick [21], where a mean-field theory of the Ising spin glass with infinite range interactions was developed before experimental discovery of reentrant transitions. They found, in particular, that in a partially frustrated system where the FM interactions prevail over the AFM ones, both FM and SG orders can be observed in different temperature intervals. In this case the FM order parameter gradually grows as the temperature is lowered starting from T_C, then passes through the maximum, and eventually vanishes at T_{RSG}. Therefore, a true RSG phase was predicted to form. The magnetic structure of this phase was found to be similar to that existing in fully frustrated SG systems at $x > x_c$. However, subsequent more realistic theories, computer simulations, and structural investigations have shown that the structural arrangement of the RSG state is typically more complex than in the ordinary spin glass with balanced FM and AFM bonds, and the spin glass and the FM (or AFM) orders may coexist at $T < T_{RSG}$.

Figure 23.3 presents schematically some microscopic models that have been considered in the literature to describe the evolution of the structure of RSG system with temperature. Snapshots of spin configurations are shown in the paramagnetic phase at temperatures well above T_C (upper part of the figure), in the FM phase well below T_C (middle part), and in the RSG phase well below the glassy freezing temperature (bottom part). Red and black arrows represent the dynamic spins whose directions vary with time and the static spins whose motion is frozen due to partially frustrated interspin interactions, respectively. The first of these models (which is referred to as the transverse or *xy* freezing model) suggests that below T_C the motion of spins becomes partially correlated, that is all of them undergo precession around a single *z* direction. In other words, the spin possesses a static component along the *z* axis and a rotating component in the perpendicular *xy* plane. This magnetic structure has a macroscopic magnetic moment, but the spontaneous magnetization is smaller than that which would exist in the same material in the case of collinear ordering characteristic of the "normal" FM phase. In this picture the subsystem of dynamic spin components fluctuating in the *xy* plane can be considered as a two-dimensional spin glass, which freezes at the transition temperature T_{RSG} (for this reason the temperature T_{RSG} is often designated in the literature as T_{xy}). Below T_{RSG}, that is in the RSG phase, the spins are completely frozen, but the ideal FM collinearity is still absent: the macroscopic spontaneous magnetization in the RSG phase remains the same as in the high-temperature FM phase (more precisely, the magnetization slowly increases upon cooling through T_{RSG} without any anomalies). This behavior has been confirmed by Monte Carlo simulations performed on a three-dimensional Heisenberg model with moderately frustrated nearest-neighbor interactions [22]. It can be seen from the above consideration that the reentrant phase in the *xy* model is not truly reentrant, as the degree of disorder does not increase when the system enters this phase. The FM order parameter is preserved and, furthermore, the transverse glassy order parameter appears; thus the resulting state can be characterized by a mixed (ferro-glass) phase where FM and SG orders coexist.

An alternative model has been proposed to explain neutron scattering experiments [17, 23]. It is sketched in the right-hand part of Figure 23.3. The model is based on the fact that in many materials the critical concentration x_c is close to the percolation threshold

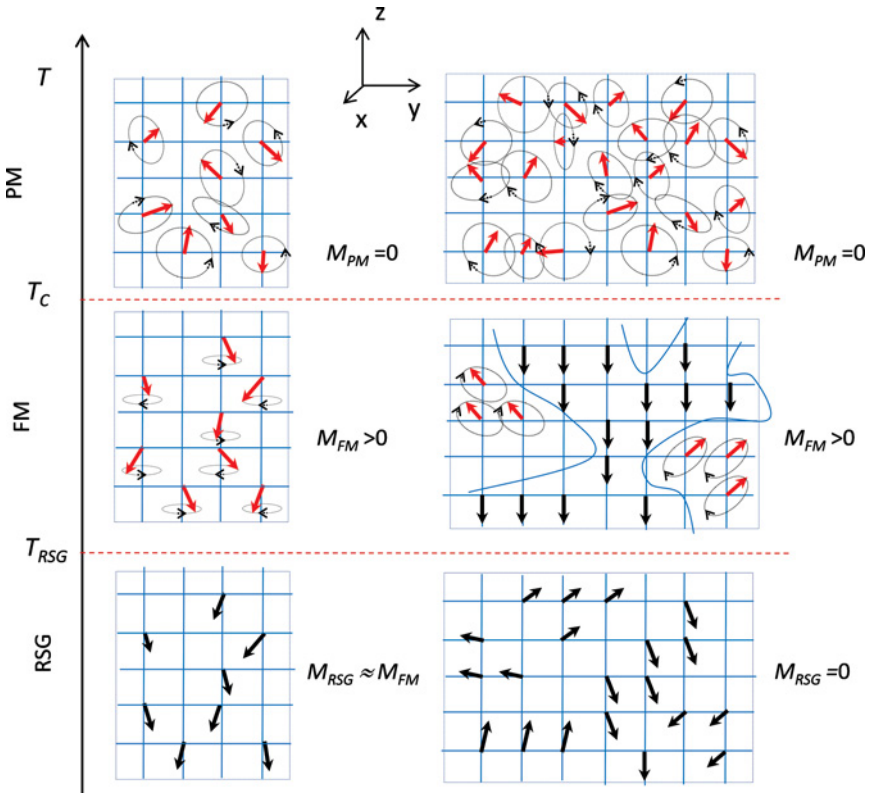

Figure 23.3 *Schematic diagram of the models explaining the RSG behavior: transverse (xy) freezing model (left-hand column) and random-field model (right-hand column). The dynamic and frozen spins are shown by red and black thick arrows, respectively. Infinite FM cluster in the FM phase of the random-field model is outlined. For a color version of this figure, see color plate section*

below which an infinite network of magnetic atoms coupled by the FM interactions cannot be obtained. The spin concentration in an RSG material is believed to be near, but above the percolation threshold. As the temperature decreases through T_C the system becomes decomposed into two intertwined networks: the first one is the static infinite FM cluster and the second one is a set of dynamic finite FM clusters and isolated spins. In entirely ferromagnetic dilute systems without frustrated interactions, the FM phase survives down to near-zero temperature (e.g. in $Mn_xZn_{1-x}F_2$; see Cowley et al. [24]). In the systems with a frustration resulting from, for example, competing FM/AFM first and second neighbor exchanges or the long-range Ruderman–Kittel–Kasuya–Yosida (RKKY) interactions, the spins outside the infinite FM cluster form a spin cluster glass environment. Further evolution of the system is determined by the interaction between these two networks and generally does not imply a true spin-glass transition at T_{RSG} in the sense of the Edwards–Anderson notation. The spins belonging to the SG network can interact with each other and with the

infinite FM cluster via different types of interactions including the long-range (dipole and RKKY) and the short-range ones, and the interactions are supposed to be frustrated [17]. This implies a glassy slowing down of spin dynamics in the SG network when approaching T_{RSG} from above. When the relaxation time becomes large and spins are effectively frozen, the fields of long-range interactions act as static random fields on the infinite FM cluster. The static random fields conjugate to the order parameter, even if they are arbitrarily weak, are able to destroy the long-range order in the Heisenberg-type system [25]. According to the "random field" model for reentrant spin glasses [17, 23], this happens at T_{RSG}, and, as a result, the macroscopic FM moment of the infinite FM cluster vanishes. This behavior has been reproduced, in particular, in the Monte Carlo simulation of a dilute classical Heisenberg model with FM nearest neighbor and AFM next-nearest neighbor interactions [26]. It was found that in the RSG phase the infinite FM cluster is broken into FM clusters [26,27], which is an expected result of random local fields. Therefore, in contrast to the transverse freezing model, where the FE order does not change at T_{RSG} but coexists with the glassy order in the RSG phase, in the random field model the FE long-range order is absent at low temperatures; that is the RSG phase is a truly reentrant one.

The random field model has been ruled out in many materials based mainly on investigations combining Mössbauer spectroscopy and spontaneous magnetization measurements (see Ryan [19] for a review). It was argued [19] that as the magnetic properties of all FM-RSG systems are essentially identical, in all cases just the transverse degrees of freedom become frozen at T_{RSG}. However, the random field model is still in use and has found experimental support in a number of materials [27–29].

The *xy* model is not compatible with the Ising magnets as the transverse spin components are impossible there and only longitudinal ordering can be observed. Nevertheless, the coexistence of longitudinal spin-glass and long-range AFM orders has been found in the RSG phase of a dilute Ising antiferromagnet, $Fe_{0.55}Mg_{0.45}Cl_2$ (the susceptibility of this material is shown in Figure 23.2). It was suggested [18] that some spins are ordered within an infinite AFM cluster and some spins are isolated or assembled into isolated finite clusters. The spins not belonging to the infinite cluster become frozen like a spin glass at low temperature. Therefore, in contrast to the *xy* model where the coexisting FE and glassy subsystems are associated with the same atoms (they are just different components of the spins), the spin system in this model is decomposed in space into two phases: a long-range ordered AFM phase and a spin-glass phase.

A similar two-phase percolation model was recently applied to antiferromagnetic complex perovskite $PbFe_{0.5}Nb_{0.5}O_3$ [30] in spite of the fact that this is the Heisenberg-type material and the transverse spin ordering is allowed here. This material is especially interesting in the context of the present review, as it is a multiferroic showing an FE phase transition concomitant with a weak relaxor ferroelectric behavior at ~380 K, a transition from a paramagnetic to an AFM phase at $T_N \approx 150$ K and the RSG behavior below ~12 K. However, a subsequent investigation combining Mössbauer spectroscopy and neutron diffraction experiments [31] ruled out the magnetic phase separation but rather revealed a freezing of a transverse spin component similar to that considered in the *xy* model. An additional feature of this system, besides the AFM order in the intermediate magnetic phase instead of FM order, is that the magnetization of the AFM sublattice slightly decreases upon cooling through T_{RSG}, i.e. the spins experience an additional canting.

23.3 Relaxor Ferroelectrics

Relaxor ferroelectrics are often considered as an electric analog of magnetic spin glasses because they exhibit similar features, such as a quenched disorder in the structure, frustrated interactions, ultra-slow relaxation dynamics, phase transition to a glassy phase under conditions far from equilibrium, aging, rejuvenation and memory effects, etc. However, a striking contrast is that, while spin glasses are basically useless as materials for practical applications, a wide range of applications has been found for relaxors due to their peculiar physical properties (giant piezoelectric effect in the FE phase, large electrostriction and high electric permittivity in the ER phase, etc.). On the other hand, while the theoretical spin-glass models are rather well developed and the behavior is generally understood, comprehensive understanding of the relaxor behavior is still the subject of intensive ongoing investigations and seems to require conceptually more complex models.

The properties of relaxors, the peculiarities of their structure, and the theoretical approaches proposed to explain their behavior have been discussed in a number of recent reviews [32–38]. Therefore, in this section we will present only briefly some basic information that is helpful in understanding the core of this chapter. Emphasis will be placed on the dielectric properties, in particular the dielectric dispersion, which conveniently provides the basic criteria to qualify a material under investigation as a relaxor.

The necessary structural condition for the appearance of relaxor behavior is the quenched (i.e. static at all relevant temperatures) compositional disorder. For example, in the prototypical relaxor $Pb(Mg_{1/3}Nb_{2/3})O_3$ (PMN), the cations Mg^{2+} and Nb^{5+} are partially disordered in the B-sublattice of the perovskite ABO_3 structure. Relaxors belong to the family of ferroelectric materials as their behavior originates from the cooperative FE-type interactions that lead to the development of (local) spontaneous polarization in the ER and NR phases. However, due to the presence of quenched compositional disorder a homogeneous polarization cannot be developed. Instead, the structure comprises nanosize clusters of unit cells with collinear (or nearly collinear) dipole moments, which form the "islands" of spontaneous polarization (i.e. PNRs). The PNRs are surrounded by a non-polar medium where the dipole moment directions of unit cells remain random. Structural data suggest that in PMN the volume fraction of the PNRs steadily increases from 0% in the PE phase to ~30% in the NR phase [39], while their size grows from ~1.5 nm (i.e. about four unit cells) in the ER phase to ~6 nm in the NR phase [40]. The structural difference between relaxors and simple dipole glasses (such as doped alkali halide crystals KCl:OH or KCl:Li) is that in the latter no dipolar clusters are formed and all unit cell dipole moments are randomly directed.

To account for the dielectric properties of relaxors, the PNRs are usually considered as large "molecules". Their thermally activated reorientations provide the main contribution to the dielectric permittivity ($\varepsilon = \varepsilon' - i\varepsilon''$) in the temperature range of the characteristic relaxor $\varepsilon(T)$ peak. The examples of this peak are presented in Figure 23.4, which shows the behavior in PMN and in the PMN–PT solid solution (PT stands for ferroelectric $PbTiO_3$). In both crystals the transition from the paraelectric to the ER state is observed at practically the same temperature $T_B \approx 630$ K, but the low-temperature behaviors are different. In PMN–PT the transition to an FE phase can be clearly seen due to the sharp drop in the $\varepsilon(T)$ curve at the Curie point $T_C = 410$ K. In some other materials the drop can be not so sharp, signifying that the ER–FE transition is

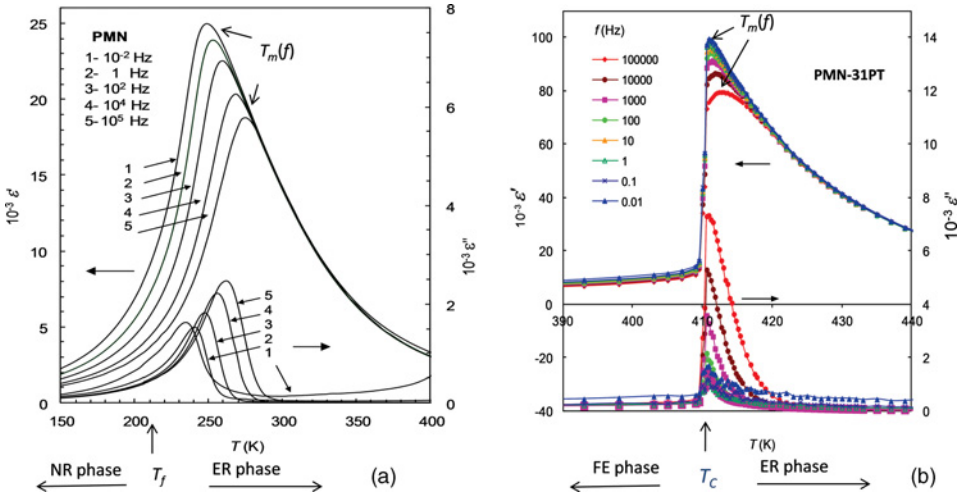

Figure 23.4 *Temperature dependences of the dielectric permittivity (a) in a canonical relaxor $Pb(Mg_{1/3}Nb_{2/3})O_3$ crystal and (b) in a crystal with relaxor-to-ferroelectric phase transition, $0.69Pb(Mg_{1/3}Nb_{2/3})O_3$–$0.31PbTiO_3$, measured at various frequencies. Reproduced from [34] with kind permission from Springer Science and Business Media*

diffuse [41]. In PMN no FE phase is developed. Instead, the phase transition to the glassy NR phase occurs at $T_f \approx 210$ K, which is not accompanied by any noticeable $\varepsilon(T)$ anomaly. In both cases, however, the temperature dependence of permittivity peaks at a frequency-dependent temperature T_m in the ER phase and a pronounced dielectric dispersion is observed around T_m. The dispersion range starts from the phonon frequencies and can spread (in canonical relaxors) down to the lowest measurement frequency available in a laboratory. This behavior contrasts with the behavior in normal ferroelectrics, where the intrinsic relaxation is observed at very high frequencies and disappears when the frequency decreases down to the MHz range.

Similar to a normal FE phase the low-temperature phase of relaxors is nonergodic, that is different configurations of elementary dipoles in the structure can have the same free energy. However, in the FE phase the non-ergodicity is much simpler. In an ideal FE crystal every elementary dipole (the dipole associated with a unit cell) can be in one of a few degenerate states prescribed by the crystal symmetry. For example, in the rhombohedral FE phase (the ground state of classical ferroelectric $BaTiO_3$) there are eight dipole configurations with the same free energy: in each configuration all the elementary dipoles are oriented along the same <111> crystallographic direction of the paraelectric cubic structure. This behavior is the consequence of FE-type interactions between elementary dipoles. In relaxors the FE interactions are local and promote correlations within PNRs only. In the temperature range of the ER–NR transition the PNRs themselves play the role of elementary dipoles. The interactions between them are believed to be frustrated (i.e. both the FE- and AFE-type couplings are present) and lead to the phase transition (cooperative freezing of thermally activated reorientations of PNR dipole moments and appearance of the Edwards–Anderson-type order parameter) at T_f.

While the concept of PNRs is consistent with many experimental results and theoretical considerations, some researchers have questioned about their existence in lead-containing perovskite relaxors [42–44]. Their arguments are based, in particular, on the results of synchrotron diffuse scattering and molecular dynamic simulations. On the other hand, first-principle-based Monte Carlo simulations in lead-free perovskite relaxors clearly point to the presence of PNRs [45]. Recent X-ray fluorescence holography experiments performed in the ER phase of PMN [46] reveal that PNRs indeed exist in lead-containing relaxors, but the traditional picture of the dipole arrangement was oversimplified. In fact, not all elementary dipoles inside PNR appear to be correlated.

Like in normal ferro- and antiferroelectrics, the static dielectric permittivity, $\varepsilon_s \equiv \varepsilon(f = 0)$ in the paraelectric phase of relaxors (i.e. at $T > T_B$) follows the Curie–Weiss law:

$$\varepsilon_s(T) = \frac{C}{T - T_{CW}} + \varepsilon_0 \tag{23.1}$$

where C and ε_0 are constants having the same meaning and the same order of magnitude as in normal ferroelectrics, while T_{CW} is significantly larger than T_m and coincides (at least approximately) with another characteristic temperature T^* (see Dkhil et al. [47] for a discussion concerning this recently discovered characteristic temperature). In the ER phase the temperature dependence of static permittivity typically has the shape of the Lorentz function [48]:

$$\frac{1}{\varepsilon_s(T)} = \frac{1}{\varepsilon_A} + \frac{(T - T_A)^2}{2\varepsilon_A \delta^2}$$

where ε_A is the value of ε_s at the maximum temperature $T_A \leq T_m(f)$ and δ (called sometimes the diffuseness parameter) is the half-width of the Lorentz ε_s (T) peak at two-thirds of the maximum. For a particular material this equation can be verified directly by fitting the data at $T > T_m$, where the dispersion is negligible and, therefore, the static permittivity is measured. Around T_A the dispersion is typically observed down to the lowest measurement frequencies and ε_s cannot be measured directly. It can, however, be derived by appropriate extrapolation of the isothermal relaxation spectra (see, for example, Bokov and Ye [49]).

The relaxation spectrum of relaxors typically comprises several contributions related to different microscopic mechanisms. In canonical relaxors the main dielectric contribution (appearing in the ER phase and dominating in the temperature range around T_m) is typically characterized by the broadening of the relaxation spectrum on cooling and the characteristic relaxation time (τ), which increases faster than the classical Arrhenius law prescribes. In the whole temperature interval where τ can be measured, it follows the Vogel–Fulcher (VF) law, which is well known in the physics of glassy systems:

$$f_r(T) = f_0 \exp\left(-\frac{E_a}{T - T_f}\right) \tag{23.2}$$

where $f_r = 1/(2\pi\tau)$ is the characteristic relaxation frequency, f_0 and E_a are the attempt frequency and activation energy of the relaxation process, respectively, and T_f is the freezing temperature at which τ tends to be infinite. Below this temperature the corresponding relaxation dynamics is supposed to be essentially frozen, which means that at $T < T_f$ the system is non-ergodic, that is T_f delimits the NR and ER phases. Similar to the orientational polarization in ordinary dielectrics the attempt frequency in relaxors typically corresponds to the

frequency of optic phonons ($\sim 10^{12} - 10^{13}$ Hz). However, in many relaxors the VF relation (23.2) does not hold and in some others a freezing temperature $T_f = 0$ K is found, which suggests that the canonical NR phase is not achieved.

A different relation has been found virtually in all relaxors within a particular frequency interval. It looks very similar to Equation (23.2) and is also referred to in the literature as the VF law:

$$f = f_m \exp\left(-\frac{E_m}{T_m(f) - T_{VF}}\right) \tag{23.3}$$

where f is the measurement frequency, T_m is the (frequency-dependent) temperature of the $\varepsilon'(T)$ or $\varepsilon''(T)$ maximum, while f_m, E_m, and T_{VF} are the empirical parameters that generally have no physical meaning. In the literature they are often erroneously associated with the attempt frequency, activation energy, and freezing temperature, respectively. Such a misunderstanding arises from the assumption that the positions of the permittivity maxima correspond to the condition $2\pi f\tau(T = T_m) = 1$ and, therefore, the $\tau(T)$ behavior and the relaxation parameters can be derived from the $T_m(f)$ curves. It is, however, known that this condition is often not satisfied in real materials (see p. 103 in Jonscher [50]). In relaxors it can be violated for two reasons. Firstly, several relaxation mechanisms with different parameters often contribute to the $\varepsilon(T)$ maximum and influence T_m. Secondly, the value of T_m at a particular f is determined not only by the relaxation time but also by the behavior of static permittivity, which is strongly temperature dependent in relaxors: it typically has the diffuse Lorentz-shaped maximum at $T_A < T_m$ (see above). As shown theoretically by Tagantsev [51], due to the maximum, Equation (23.3) can be satisfied in some frequency range even when Equation (23.2) does not hold. This can happen under the condition that the relaxation spectrum broadens gradually upon cooling (as often happens in relaxors). Recent numerical simulations showed [49] that the latter condition is not necessary and the relation (23.3) with $T_{VF} > 0$ can be observed even when the relaxation time follows the Arrhenius law and the shape of the spectrum does not change with temperature.

The values of f_m reported for different relaxor materials fall into a wide frequency range of $10^6 - 10^{16}$ Hz or so, and can be very different for the same material when derived from the $\varepsilon'(T)$ and $\varepsilon''(T)$ curves or at different frequency intervals. In canonical relaxors where the freezing of the dielectric spectrum does occur and the relaxation frequency follows the VF law (23.2), the relations $f_{mRe} \approx f_{mIm} \approx f_0$, $E_{mRe} \approx E_{mIm} \approx E_a$, and $T_{VFRe} \approx T_{VFIm} \approx T_f$ are usually satisfied (the subscripts Re and Im denote the parameters derived from the $\varepsilon'(T)$ and $\varepsilon''(T)$ dependences, respectively).

Equation (23.3) can be easily verified in experiment as the temperatures $T_m(f)$ are clearly seen in the $\varepsilon(T)$ curves. On the contrary, verification of Equation (23.2) is often a complicated task. In particular, it requires the analysis of the dielectric spectra (isothermal frequency dependences of permittivity) typically consisting of several overlapping contributions, which should be properly separated.

A large enough external electric field applied to a canonical relaxor at $T < T_f$ can induce irreversibly the FE phase with $T_C = T_f$. The question whether this phase is stable or metastable is under discussion in the current literature, but it can only be destroyed by heating the sample to $T > T_C$. This feature distinguishes relaxors from dipolar glass or spin glass where the field-induced collinear order is unstable. The macroscopic properties of the FE phase in relaxors (canonical and non-canonical) are quite similar to the properties

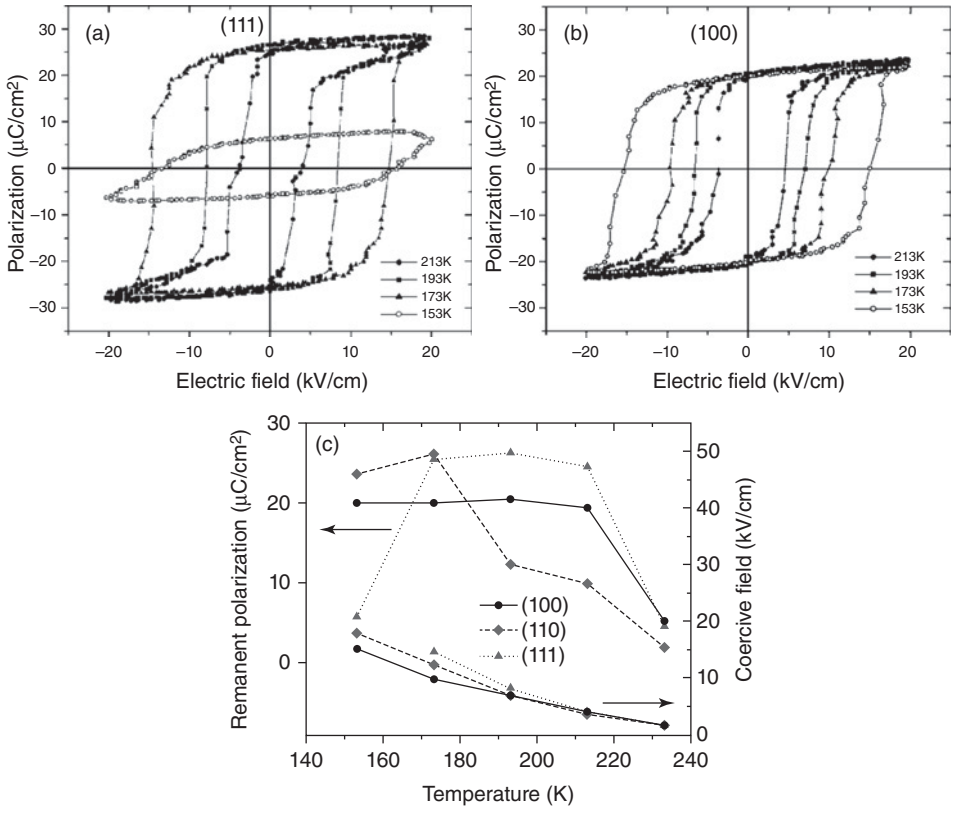

Figure 23.5 *Ferroelectric hysteresis loops displayed in the NR phase of $Pb(Mg_{1/3}Nb_{2/3})O_3$ crystal in different crystallographic directions: (a) along [111] and (b) along [100], and (c) the temperature dependences of the remanent polarization and coercive field obtained from these loops. Reprinted (Figures 5(a) and (c) and 6) from [52] with permission from Zhao et al. Copyright (2007) by the American Physical Society*

of the FE phase in normal ferroelectrics. In particular, piezo- and pyroelectric effects are observed. Due to the possibility to induce the FE phase, typical rectangular-shaped ferroelectric $P(E)$ hysteresis loops are observed in the NR phase (in contrast to the opinion expressed in some papers that the hysteresis loops in relaxors are slim). The examples are presented in Figure 23.5 showing the loops in the NR phase of the PMN crystal. Note that in Figure 23.5(c) the temperature dependence of the *measured* remanent polarization (P_r) in the [111] direction reveals a maximum and P_r almost disappears at low temperatures. This looks like a reentrant behavior, but it is not the case. In fact, the low-temperature drop of P_r is a result of the increase in the coercive field to the level above the measurement field rather than a real anomaly in the T dependence of the spontaneous polarization. This is clear, in particular, from the $P_r(T)$ dependence measured in the [100] direction in which the coercive field is smaller, the loops are saturated, and the measured P_r (T) reflects the true behavior of the spontaneous polarization. The latter is practically temperature-independent at low temperatures. Note that the similar problem was discussed (see Section 2.2 in Ryan [19]) in

the field of magnetic materials where the maximum in the temperature dependence of zero-field-cooled magnetization was erroneously interpreted by some researchers as the sign of a reentrant transition; it is in fact the result of anisotropy, which exceeds the measuring field.

When discussing the reentrant behavior in relaxors, a number of essentially different situations need to be considered. The first one is the paraelectric–ferroelectric–relaxor sequence of phases upon cooling. In this case the characteristic relaxor-type dielectric dispersion appears at temperatures below a rather sharp dielectric peak associated with the FE Curie point. Alternatively, the notion of reentrant glass (not reentrant relaxor) behavior is applied to describe a more subtle situation where some properties of relaxors (in particular, aging and Barkhausen noise) are apparently similar to the properties of reentrant *xy* spin glasses. This type of behavior can be found even in canonical relaxors, such as PMN, that is in materials where the FE phase is not observed at all under zero-field cooling conditions. Finally, a transformation to the reentrant dipolar glass state has been reported in doped quantum paraelectrics in which relaxor and/or FE transformations have also been observed at higher temperatures. All these scenarios are reviewed separately in the following sections.

23.4 Reentrant Relaxor Behavior in Ferroelectrics

As discussed in the previous section, the typical sequences of phases in relaxor materials are PE–ER–NR or PE–ER–FE. In the former case, a smooth and dispersive diffuse maximum is observed in the temperature dependence of dielectric permittivity at $T_m(f)$. In the latter case a more or less distinct anomaly appears additionally below T_m. The temperature of this anomaly is practically independent of frequency and corresponds to a sharp or diffuse transition to an FE phase. However, some exceptions are known when the temperature $T_m(f)$ of the relaxor-like $\varepsilon(T)$ anomaly is lower than T_C. Recently, this kind of behavior has attracted a great deal of attention. Questions have been raised and discussed as to whether the state below T_m can be considered as a distinct reentrant relaxor phase and what the possible microscopic mechanisms of the phenomenon are.

When considering the origin of reentrant-type relaxor dispersion, the first point to check is the macroscopic homogeneity of the sample. FE crystals and ceramics are often complex compounds or solid solutions, in which inhomogeneities related to composition segregation or regions of different compositional disorder can be expected. In these cases the anomalies of properties at T_m and T_C might be associated with the chemically different mesoscopic or macroscopic regions of the material.

Another possibility is that some extrinsic dielectric contributions can be responsible for relaxor-like dielectric anomalies in the FE phase. Inhomogeneities due to ceramic grain boundaries or material/electrode interfaces often lead to the Maxwell–Wagner-type dielectric response with a very large (up to $\sim 10^5$) dielectric susceptibility and with dielectric dispersion in the frequency range routinely used for dielectric measurements. Significant extrinsic dielectric response may also come from the relaxation of FE domain walls. A noticeable example is given in Figure 23.6, which shows the temperature dependence of the dielectric permittivity in the low-temperature phases of a crystal of the classical ferroelectric $BaTiO_3$. The sharp maxima observed at 180 K and 270 K are caused by rhombohedral–orthorhombic and orthorhombic–tetragonal phase transitions, respectively (the Curie point is located at 440 K outside the range shown in the figure). There are no phase transitions

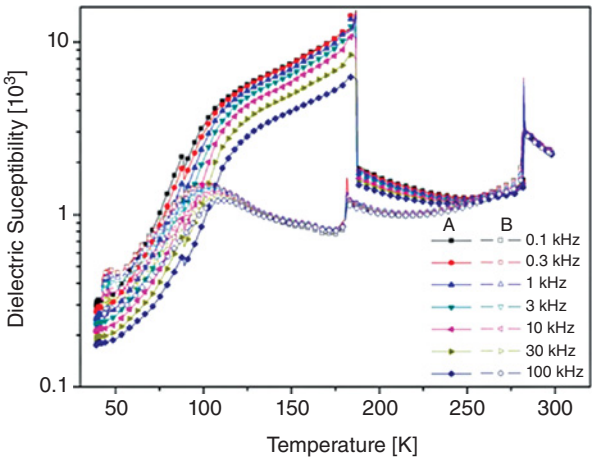

Figure 23.6 *Temperature dependence of small-signal dielectric permittivity of two <111>$_{cub}$ oriented $BaTiO_3$ single crystals. Before measurements sample A was electrically depoled at room temperature with a fast-decayed (from 1 kV/cm to zero within five periods) low-frequency AC field and sample B was annealed at 450 °C for 10 h. Reprinted from [53] with permission from Wang et al. Copyright [2011], AIP Publishing LLC*

below 180 K in this crystal, but a pronounced dielectric anomaly is observed at around 100 K, whose shape and magnitude resemble the behavior of relaxors. In particular, in the crystal annealed at $T > T_C$ (open symbols in Figure 23.6) one can see the diffuse $\varepsilon(T)$ peak with dispersion on the low-temperature slope and the frequency-dependent T_m, similar to the peak typically observed at temperatures above the ER–NR transformation. However, one can hardly expect a relaxor phase in $BaTiO_3$ because the compositional disorder that is a necessary condition for relaxor behavior to occur is absent. Accordingly, the structure of the low-temperature state and the mechanism of the dispersion are completely different from those observed in canonical relaxors. It was shown [53] that the relaxation in the rhombohedral phase of $BaTiO_3$ is related to the motion of the walls of macroscopic FE domains rather than to the dynamics of PNRs. The intrinsic (single-domain) permittivity is comparatively small (~100) and decreases monotonically on cooling in the rhombohedral phase [54]. Accordingly, the dielectric behavior is highly dependent on the domain structure: samples A and B in Figure 23.6 were shown (by means of transmission electron microscopy) to possess very different domain wall densities and configurations.

Below we will discuss examples of reentrant relaxor behavior in such materials where compositional disorder exists and, therefore, relaxor phases can be expected.

23.4.1 Properties of Materials with Paraelectric–Ferroelectric–Relaxor Sequence of States

23.4.1.1 Ferroelectrics with Perovskite Structure

The term "reentrant relaxor" was first applied to a novel perovskite solid solution (1 – x)$BaTiO_3$–$x AgNbO_3$ (BT–AN) whose end members are the classical ferroelectric BT and

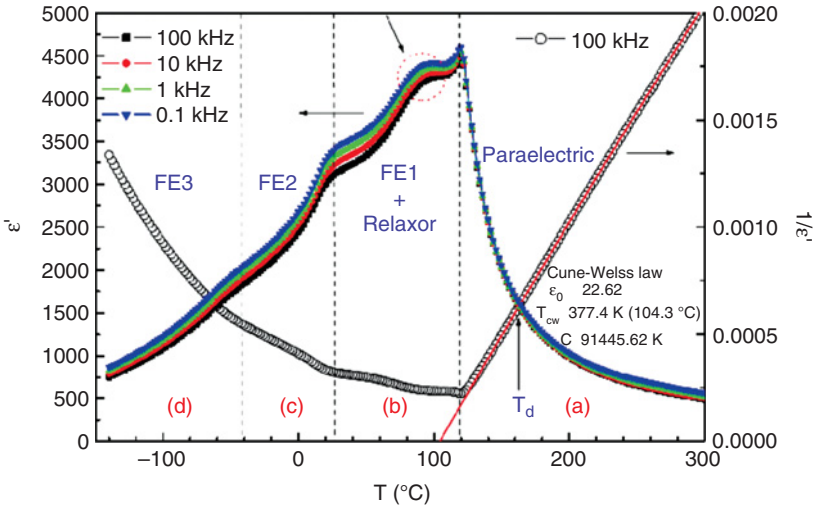

Figure 23.7 *Temperature dependences of the dielectric permittivity at different frequencies and the reciprocal of the dielectric permittivity at 100 kHz of the $0.99BaTiO_3$–$0.01AgNbO_3$ ceramics. Solid line is the fit to the Curie–Weiss law, Equation (23.1). From [55]. © IOP Publishing. Reproduced by permission of IOP Publishing. All rights reserved*

the antiferroelectric (at low temperatures) AN [55]. Ceramic samples with $x \leq 0.1$ were prepared and studied [55, 56]. The room-temperature unit cell volume determined using X-ray powder diffraction increased linearly with increasing x while the tetragonality decreased, that confirmed the formation of the solid solution. In all compositions the paraelectric—ferroelectric phase transition was observed almost at the same temperature $T_C \approx 120$ °C as in the pure BT. In Figure 23.7, which shows the temperature dependence of the dielectric permittivity of the 0.99BT–0.01AN ceramics, this transition is clearly seen as a sharp peak. As expected for a normal phase transition, the position of the peak is frequency independent. The anomaly at 25 °C corresponds to the transition from the high-temperature FE phase of tetragonal symmetry (FE1) to the FE orthorhombic (FE2) phase. At –40 °C the FE2 phase transforms into the rhombohedral FE3 phase (the same phase sequence is known to occur in pure BT). However, an additional distinct dielectric anomaly is seen at about 100 °C whose temperature depends on frequency and, therefore, it can hardly be associated with a normal phase transition. With increasing x this anomaly shifts to lower temperatures and becomes much more pronounced, transforming into a diffuse maximum, while the peak at T_C decreases in magnitude, and in the compositions with $x > 0.02$, it is visible only as a comparatively small kink at the high-temperature side of the main diffuse $\varepsilon(T)$ peak [56].

The transition at T_C demonstrates the features characteristic of the normal FE Curie point [55]: in particular, the permittivity at $T > T_C$ follows the CW law with $T_{CW} < T_C$ (see Figure 23.7), the differential scanning calorimetry (DSC) reveals a thermal anomaly at T_C, and the spontaneous polarization (derived from FE hysteresis loops) appears below T_C. On the other hand, in the temperature range of the additional dielectric anomaly at 100 °C no anomalies

are observed in the DSC curves or in the temperature dependences of remanent polarization (the behavior characteristic of relaxors). Furthermore, in the frequency range of 400 Hz–1 MHz the temperature of the anomaly follows the VF law for T_m, Equation (23.3), which is a hallmark of relaxor behavior. The best-fit parameters are $f_{mRe} = 9 \times 10^9$ Hz, $E_{mRe}/k = 0.0096$ eV, and $T_{VFRe} = 365$ K. However, it remains unclear whether freezing of the dielectric spectrum actually takes place. The verification of the VF law for the relaxation time, Equation (23.2), appears to be practically impossible due to the complexity of the relaxation spectrum (with the relaxation mechanisms overlapping in frequency). The observed value of f_m is seemingly too low to be considered as the attempt frequency of a relaxor-type dispersion. Besides, in the BT–AN ceramics with $x = 0.1$ [56] the parameters of Equation (23.3) determined from the $\varepsilon'(T)$ and $\varepsilon''(T)$ peaks differ significantly ($f_{mRe} = 9 \times 10^{14}$ Hz, $f_{mIm} = 7 \times 10^{10}$ Hz, $E_{mRe}/k = 0.084$ eV, $E_{mIm}/k = 0.064$ eV, $T_{VFRe} = 154$ K, and $T_{VFIm} \approx 98$ K), which is not typical of canonical relaxors.

The reentrant-like behavior of BT–AN was attributed [56] to the compositional segregation: mesoscopic regions with $x = 0$ were supposed to be responsible for the sharp maximum at ≈120 °C, while the diffuse anomaly at ≈100 °C was due to Ag-rich regions. This interpretation was supported by X-ray diffraction experiments: a mixture of the tetragonal phase and the cubic phase having smaller unit cell volume was observed between ∼100 °C and T_C in 0.99BT–0.01AN, while pure tetragonal and cubic phases were found below and above this temperature interval, respectively. It was further proposed that the inhomogeneity has the form of a core–shell microstructure where the compositions of core and shell regions of a ceramic grain are different. Therefore, the state observed below the relaxor-like dielectric anomaly is an FE rather than a glassy state. This is also confirmed by the observation of macroscopic (∼1 μm in size) FE domains imaged with the piezoresponse force microscopy (PFM) at room temperature. The relaxor-like dielectric dispersion has been tentatively attributed to the domain wall relaxation and to the relaxation of the boundaries between mesoscopic paraelectric Ag-free regions and the FE phase, which is developed during the diffuse FE transition at $T < T_C$ in the regions with $x > 0$ [56]. We further suggest that the characteristic of relaxor VF law for T_m, Equation (23.3), is due to the maximum in the temperature dependence of static permittivity, which is expected to be developed at the diffuse FE transition. As discussed in Section 23.3, any dispersion may satisfy Equation (23.3) in a certain frequency interval if this maximum exists.

Another BT-based solid solution that shows a reentrant-type dielectric behavior is the $(1 - x)BaTiO_3$–$xBiScO_3$ [$(1 - x)$BT–xBS] ceramics. Similar to BT–AN considered above, in $(1 - x)$BT–xBS with a comparatively small x, the first, frequency-independent, anomaly is observed in the $\varepsilon'(T)$ dependences at $T \approx 140$ °C, approximately equal to T_C in pure BT (see Figure 23.8), and the second anomaly, observed at a lower temperature, T_m, is not related to a structural phase transition as confirmed by the DSC data [57, 58]. The relaxor-type nature of the second anomaly is suggested by the fact that T_m follows the VF relation, Equation (23.3), which was verified for both the $\varepsilon'(T)$ and $\varepsilon''(T)$ dependences. In the temperature range between T_m and T_C the material shows the typical FE characteristics, including $P(E)$ hysteresis loops, macroscopic FE domains observed with PFM and the tetragonal distortion of the perovskite unit cell (according to the X-ray diffraction data). However, with increasing x the distortion gradually decreases and in the samples with $x = 0.1$ the tetragonality almost vanishes (at room temperature) [58]. Our analysis (the details of which will be published elsewhere) of the dielectric data obtained previously [58] shows

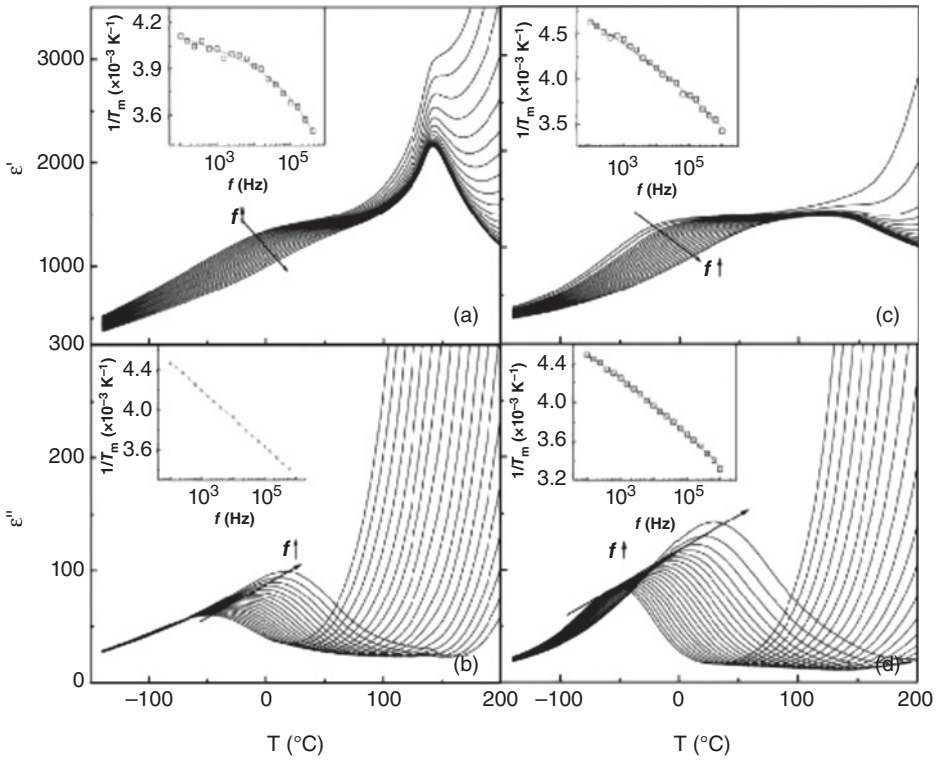

Figure 23.8 *Temperature dependences of the real (a, c) and imaginary (b, d) parts of the dielectric permittivity measured at different frequencies between 10^2 and 10^6 Hz in the $(1 - x)BaTiO_3$–$xBiScO_3$ ceramics with x = 0.05 (a, b) and x = 0.1 (c, d). Arrows indicate the direction of the frequency increase. Insets show the fitting to Equation (23.3). Reprinted from [57] with permission from Guo et al. Copyright [2008], AIP Publishing LLC*

that in the temperature range of the relaxor-type dispersion the $\varepsilon(f)$ dependences obey the Kohlrausch–Williams–Watts relaxation pattern similar to the canonical relaxor PMN. Furthermore, the characteristic relaxation time follows the VF law, Equation (23.2), with the parameters $T_f \approx 110$ K for $x = 0.1$ and $T_f \approx 160$ K for $x = 0.05$. The attempt frequency f_0 is in the phonon frequency range and the activation energy $E_a \sim (1 - 2) \times 10^3$ K is close to that in PMN. Therefore, these new results suggest the existence of a reentrant relaxor-type non-ergodic state at $T < T_f$. To the best of our knowledge, $(1 - x)$BT–xBS is the first and so far the only known material in which the reentrant relaxor dispersion is associated with a true freezing of the relaxation spectrum. However, we do not have enough information to determine what happens with the FE spontaneous polarization and what the microscopic mechanism of the relaxor relaxation is.

In the $(1 - x)$BT–xBS solid solutions with comparatively large x, only a single $\varepsilon'(T)$ maximum remains, which looks like those observed in canonical relaxors. Another canonical relaxor feature, that is the cubic macroscopic symmetry, has been revealed there by X-ray and neutron diffraction studies [59]. The glassy aging, rejuvenation, and memory effects

similar to those observed in PMN (see Section 23.5) were also found in the ceramics with $x = 0.3$ by Bharadwaja et al. [60]. However, these authors claimed significant differences between some other properties of these ceramics and the properties of canonical relaxors such as PMN. In particular, a considerable drop of remanent polarization determined from the polarization-field hysteresis loops (P_r) was found upon cooling at temperatures significantly lower than T_{VF}, which, as the authors believed, is not characteristic of PMN. Based on this difference a special "reentrant dipole glass" state was suggested to appear in $(1 - x)$BT–xBS at low temperatures. We argue that a similar low-temperature drop of P_r has indeed been observed in PMN (see Figure 23.5(c)) and explained by the increase of the coercive field above the measurement field rather than by the real drop in the spontaneous polarization. Furthermore, we have found (the details will be published elsewhere) that the VF relations (23.2) and (23.3) are fulfilled in $(1 - x)$BT–xBS with $x = 0.3$ with a freezing temperature $T_f = 151$ K and an activation energy $E_a = 0.15$ eV, which is not very different from $E_a = 0.07$ eV observed in PMN. Therefore, it seems that the $(1 - x)$BT–xBS solid solutions with large x are canonical relaxors with the transition from the ergodic to nonergodic relaxor phase at T_f similar to PMN. Further investigations are needed to examine the low-temperature behavior of remanent polarization, in particular the measurement of a possible pyroelectric current.

The relaxor phase that appears in the temperature range below the FE phase was also reported in $Ba_{0.9}Bi_{0.067}(Ti_{1-x}Zr_x)O_3$ perovskite ceramics with $x < 0.075$ [61]. However, the conclusion about the existence of the transition to the relaxor phase was only supported by the dielectric dispersion observed at $T \ll T_C$ and the FV relation which could confirm the relaxor nature of the dispersion has not been verified.

23.4.1.2 Ferroelectrics with Tungsten Bronze Structure

Besides the perovskite compounds that represent the most widely studied family of ferroelectric materials, ferroelectricity as well as relaxor behavior is also observed in materials with a tungsten bronze structure. However, in contrast to perovskites whose paraelectric phase is cubic, the paraelectric phase of the tungsten bronze compounds generally possesses a centrosymmetric tetragonal *4/mmm* symmetry. They are typically uniaxial ferroelectrics with the tetragonal *4mm* or orthorhombic FE phase. Besides the permittivity maximum observed at the ferroelectric T_C, another $\varepsilon(T)$ peak has been found in many tungsten bronze ferroelectrics at much lower temperatures. This peak was accompanied by the dielectric dispersion which led to the frequency shift of T_m in a similar way as in relaxors. However, for a long time this behavior had not been identified as a reentrant relaxor. Only recently was this identification applied to several tungsten bronze materials including $Ba_2Pr_xNd_{1-x}FeNb_4O_{15}$ [62, 63] and $Sr_2NaNb_5O_{15}$ [64].

$Ba_2Pr_xNd_{1-x}FeNb_4O_{15}$ is a solid solution composed of $Ba_2PrFeNb_4O_{15}$, which is a relaxor with $T_m \sim 170$ K (see Figure 23.9), and $Ba_2NdFeNb_4O_{15}$, which is a ferroelectric with $T_C = 323$ K. In the $Ba_2Pr_xNd_{1-x}FeNb_4O_{15}$ ceramics with $0.2 \leq x \leq 0.8$ the reentrant-type coexistence of FE phase transition and relaxor $\varepsilon(T)$ maximum was found [62]. In the T–x phase diagram of the solid solution (Figure 23.10) both T_C and T_m are nearly independent of the composition and the dielectric anomaly related to the FE phase transition and the low-temperature relaxor peak simply disappear at x close to unity and zero, respectively. The X-ray microprobe analysis of the samples showed that uncontrolled phase segregation

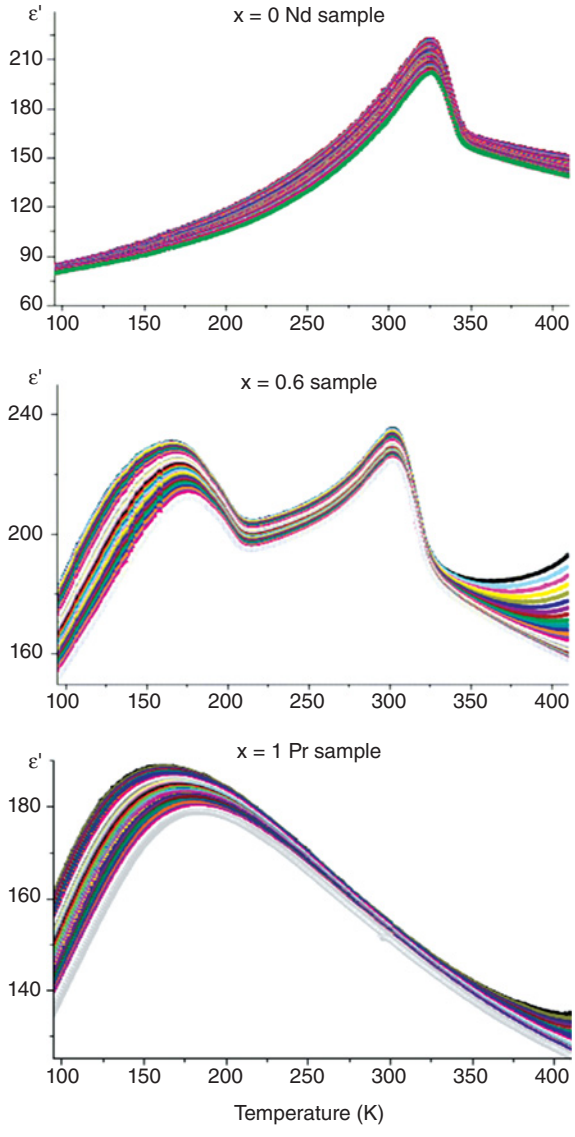

Figure 23.9 *Temperature dependences of the dielectric permittivity of the* $Ba_2Pr_xNd_{1-x}FeNb_4O_{15}$ *ceramics with x = 0, 0.6, and 1, measured on heating at different frequencies from 100 Hz (top curves) to 1 MHz (bottom curves). Reprinted from [62] with permission from Castel et al. © [2009] IOP Publishing. All rights reserved*

that could lead to this behavior is absent. The FE character of the intermediate phase was confirmed by the display of $P(E)$ hysteresis loops and the ultrasonically detected piezoelectric signal, while the observed VF law for T_m, Equation (23.3), confirmed the relaxor character of the low-temperature permittivity maximum [62, 65]. However, the freezing of dielectric spectrum (i.e. the validity of Equation (23.2)) has not been verified.

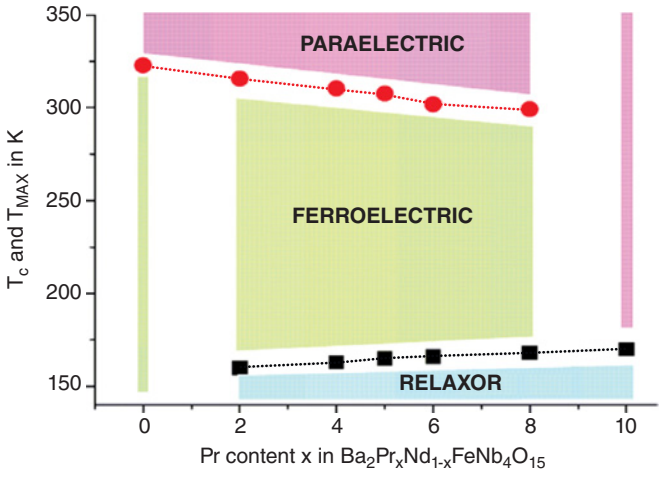

Figure 23.10 *Qualitative phase diagram of $Ba_2Pr_xNd_{1-x}FeNb_4O_{15}$ solid solution. T_C and T_m are shown by circles and squares, respectively. Reproduced from [62] by permission from rom Castel et al. © [2009] IOP Publishing. All rights reserved*

Recent measurements of the $\varepsilon'(T)$ dependences in $Ba_2Pr_xNd_{1-x}FeNb_4O_{15}$ with $0.2 \leq x \leq 0.8$ revealed no reentrant behavior upon cooling from the paraelectric phase: a single diffuse maximum was observed, which is located between the temperatures corresponding to the heating maxima [65]. This was explained by a large temperature hysteresis of T_C on cooling, which resulted in the overlap of the $\varepsilon'(T)$ peak corresponding to T_C with the low-temperature relaxor peak.

Another tungsten bronze compound where the reentrant relaxor behavior was studied in detail is $Sr_2NaNb_5O_{15}$ [64]. The shape of the temperature dependence of permittivity of this ceramic (see Figure 23.11(a)) is very similar to that observed in the above-considered $Ba_2Pr_xNd_{1-x}FeNb_4O_{15}$. The maximum at the frequency-independent temperature of 518 K corresponds to the Curie point. The dielectric permittivity above T_C obeys the CW law with the parameters of $C \sim 1 \times 10^5$ K and $T_{CW} < T_C$, characteristic of a normal PE–FE phase transition [66]. The low-temperature relaxor-like maximum at $T_m \approx 240$ K shifts with frequency according to the VF law, Equation (23.3), typical of relaxor behavior, with the parameters of $T_{VF} = 189$ K, $E_m = 1.9 \times 10^3$ K, and $f_m = 3.7 \times 10^{17}$ Hz. Interestingly, at temperatures close to T_m the anomalies of other properties were observed, suggesting that some structural changes probably occur there. In particular, the remanent and saturation polarizations determined from the well-saturated $P(E)$ hysteresis loops revealed the maximum (Figure 23.11(b)). The anomalies in elastic properties were also found: a minimum of the Young's modulus and a maximum of the mechanical loss tangent. However, the X-ray and neutron diffraction as well as the transmission electron microscopy did not reveal any structural phase transitions: the structure remained orthorhombic (space group *Im2a*) with the fully disordered arrangement of Sr and Na atoms in the whole temperature range between 100 K (the lowest examined temperature) and T_C. At the same time, the Invar effect characteristic of canonical relaxors was observed; that is as the temperature is lowered, the unit cell volume becomes temperature-independent at $T < T_m$. However, in

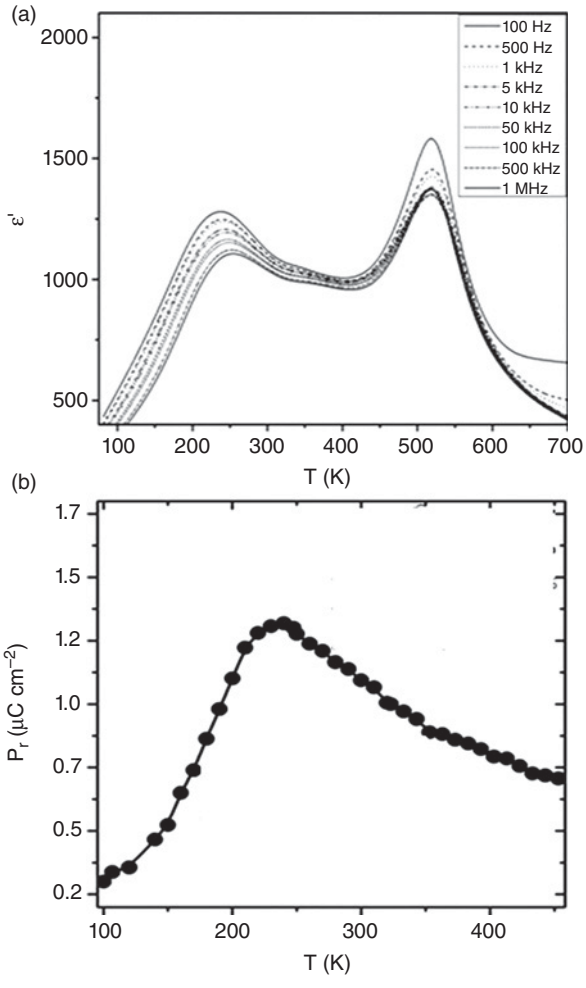

Figure 23.11 *Reentrant relaxor behavior in the $Sr_2NaNb_5O_{15}$ ceramics. Temperature dependences of (a) dielectric permittivity at different frequencies from 100 Hz to 1 MHz and (b) remanent polarization obtained from the P(E) hysteresis loops. Reprinted from [64] with permission from Torres-Pardo et al. Copyright (2011) American Chemical Society*

contrast to canonical perovskite relaxors where the structure is cubic and, therefore, a constant volume is necessarily associated with constant unit cell parameters, in $Sr_2NaNb_5O_{15}$ the orthorhombic lattice parameters a and c increase on cooling below T_m, but the increase is compensated by the decrease of b, giving rise to the Invar effect.

Recently a reentrant relaxor behavior was claimed in the $Ba_5RTi_3Nb_7O_{30}$ (R = La, Nd, Sm) ceramics in spite of the fact that a single $\varepsilon'(T)$ maximum was observed at the frequency-dependent temperature T_m [67]. It was found that the temperature dependence of remanent polarization (P_r) determined from the $P(E)$ hysteresis loops passes through a maximum at $T_r < T_m$, similar to that depicted in Figure 23.11(b). The temperature T_r was defined as a

reentrant temperature and it was suggested that below T_r the long-range FE order is broken. We note, however, that the hysteresis loops reported in this paper were very far away from saturation, especially at low temperatures. This suggests that the largest field applied was smaller than the coercive field needed to switch all the FE domains. Therefore, the measured remanent polarization was smaller than the spontaneous FE polarization and the difference between them increased upon cooling (due to an expected increase of the coercive field), giving rise to the $P_r(T)$ maximum. This explanation is supported by the fact that the increase in the maximal measurement field resulted in both a significant increase of P_r and a decrease of T_r. Therefore, similar to the situation in perovskite $(1 - x)$BT–xBS, discussed above, alternative methods for the spontaneous polarization measurement are needed to determine reliably the low-temperature behavior of the long-range FE order. Note that analysis of the pyroelectric effect in a number of different tungsten bronze crystals with the reentrant-type relaxor behavior does not reveal a $P_r(T)$ maximum, as discussed below.

To understand the origin of reentrant relaxor properties in the tungsten bronze compounds, it would be helpful to consider the results obtained on single crystals. Figure 23.12 illustrates a typical situation. In all the tungsten bronze crystals studied that exhibited the reentrant behavior, the low-temperature relaxor-type dielectric peak was found to be absent or significantly suppressed along [001] (i.e. the tetragonal c axis), but was clearly observed at $T_m < T_C$ in the directions orthogonal to [001]. On the contrary, the dielectric peak observed at T_C in the orthogonal directions is very small, or probably completely absent, as it is typically several orders of magnitude

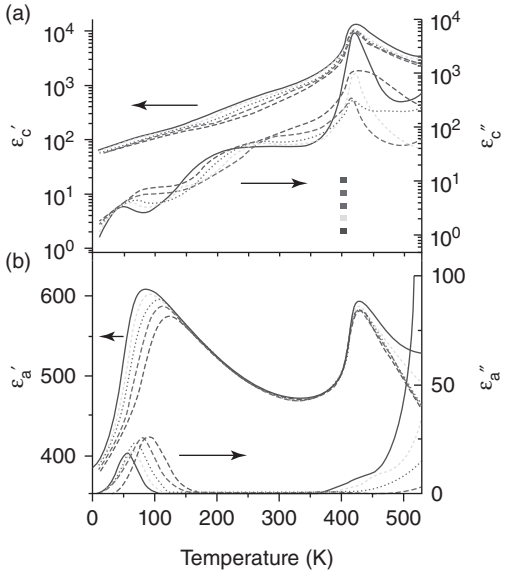

Figure 23.12 *Temperature dependences of the real and imaginary parts of dielectric permittivity in the $(K_{0.5}Na_{0.5})_{1.0}(Sr_{0.75}Ba_{0.25})_{4.5}Nb_{10}O_{30}$ crystal doped with 0.04 wt% of CuO, measured along the (a) c axis and (b) a axis of the tetragonal lattice. The probe frequencies are 0.079 (solid), 0.796 (dash), 7.96 (dot), 79.6 (dash–dot), and 796 kHz (dash–dot–dot). Reprinted from [68] with permission from Ko et al. Copyright [2002], AIP Publishing LLC*

smaller than along the polar axis, which can be explained [69] by the hardly avoidable small misorientation of the sample studied. This anisotropy was found, in particular, in the $Sr_{0.61}Ba_{0.39}Nb_2O_6$, $(K_{0.5}Na_{0.5})_{1.0}(Sr_{0.75}Ba_{0.25})_{4.5}Nb_{10}O_{30}$, $K_{5.80}Li_{3.82}Nb_{10.88}O_{30}$ [68], $Sr_{0.5}Ba_{0.5}Nb_2O_6$, $Pb_{0.37}Ba_{0.63}Nb_2O_6$, and $(K_xNa_{1-x})_{0.4}(Sr_yBa_{1-y})_{0.8}Nb_2O_6$ [70] crystals. Note that for the last composition the phase transition related to the low-temperature permittivity peak was derived from the X-ray diffraction analysis. The crystal symmetry was reported to change from the tetragonal 4*mm* to the monoclinic *m*, accompanied by the tilting of polarization away from the *c* axis of the tetragonal lattice as the temperature decreased. However, for other compositions the phase transition was not confirmed. The specific heat measurements around T_m revealed no latent heat or any significant change in the slope of the *Cp* versus *T* curve [70,71]. Analysis of the dielectric response and pyroelectric properties performed by Ko et al. [68] shows that the crystals were isotropic in the plane perpendicular to the *c* axis. In this plane the characteristic relaxation time, $\tau_r = (2\pi f_r)^{-1}$, determined from the frequency of the $\varepsilon''(f)$ maximum at fixed temperatures around T_m, was found to follow the Arrhenius law (i.e. Equation (23.2) with $T_f = 0$), while the validity of Equation (23.3) was not checked. Upon cooling the relaxation spectrum widened considerably. In $Sr_{0.61}Ba_{0.39}Nb_2O_6$, where the dielectric response was studied by means of IR reflectivity and time domain THz spectroscopy [69], no anomalies in the temperature dependences of the phonon contribution were observed. This suggests the order–disorder mechanism of the FE phase transition. The temperature dependence of the spontaneous polarization was determined in a number of tungsten bronze crystals from the pyroelectric current measurements [68, 70]. A typical result is shown in Figure 23.13, which depicts the behavior of the $(K_{0.5}Na_{0.5})_{0.4}(Sr_{0.60}Ba_{0.40})_{0.8}Nb_2O_6$ crystals. The relaxor-type peak of the dielectric permittivity is observed in the *a*-plate sample between $T_m = 58$ K (at 1 kHz) and

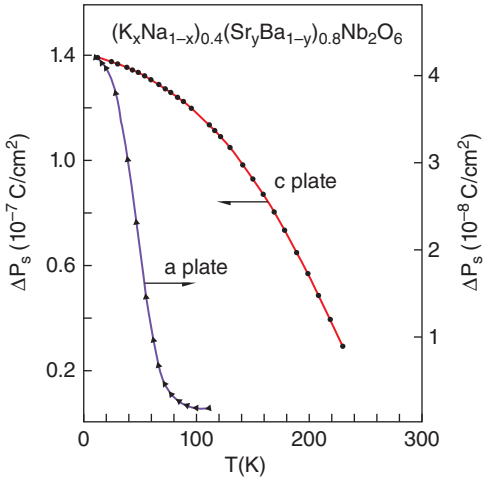

Figure 23.13 *Temperature dependences of the remanent polarization variation obtained by the measurements of the pyroelectric current in the $(K_{0.5}Na_{0.5})_{0.4}(Sr_{0.60}Ba_{0.40})_{0.8}Nb_2O_6$ crystals along the [001] (c-plate) and [100] (a-plate) directions of the tetragonal structure. Reprinted (Figure 9) from [70] with permission from Xu et al. Copyright (1989), American Physical Society*

$T_m = 76$ K (at 100 kHz). In the *c*-plate the dielectric permittivity increases smoothly with increasing temperature, as expected for a ferroelectric with $T_C > 300$ K. It can be seen in the figure that in the [001] direction the polarization gradually decreases with increasing temperature, as expected in an FE phase. In the perpendicular direction the spontaneous polarization is not expected as the symmetry is tetragonal, but the remanent polarization along <100> and <110> was found to exist at $T < T_m$ and vanished only at higher temperatures. It was shown to be practically proportional to the poling field [68], in contrast to highly non-linear behavior characteristic of ferroelectrics. Note that similar proportionality was observed in dipole glasses that show no long-range polar order at any temperature.

23.4.2 Models and Theories

Several models have been proposed to explain the reentrant relaxor behavior in macroscopically homogeneous samples. Kleemann [63] suggested that two peaks in the temperature dependence of the permittivity in $Ba_2Pr_xNd_{1-x}FeNb_4O_{15}$ (and other reentrant relaxors including perovskites) are caused by the coexistence of two phases, which is probable in the framework of percolation theory. In particular, in a solid solution with an *fcc* structure two mutually penetrating infinite percolation clusters can be formed in the composition range of $0.13 < x < 0.87$, which is consistent with the phase diagram in Figure 23.10. In one of these clusters the ferroelectric phase is developed, while the other one seems to include PNRs responsible for the relaxor behavior.

An alternative explanation was suggested in the theoretical work by Stephanovich [72], who applied a replica-symmetric solution of the disordered Ising model to describe the *T*–*x* phase diagram and FE hysteresis loops in $Ba_2Pr_xNd_{1-x}FeNb_4O_{15}$. It was believed that the low-temperature phase in the compositions with $x \geq 0.2$ is a dipole glass rather than a relaxor. This conclusion was supported mainly by the opinion that classical relaxors like PMN "never have ferroelectric hysteresis". We argue, however, that well-saturated FE hysteresis loops can in fact be displayed in PMN and other relaxors (see Section 23.3), arising from the induced ferroelectricity [32, 34]. Other proofs are required to discard the relaxor nature of the dielectric relaxation in $Ba_2Pr_xNd_{1-x}FeNb_4O_{15}$.

Schefer et al. [71] contended that high-resolution neutron powder diffraction on $Sr_{0.61}Ba_{0.39}Nb_2O_6$ reveals small changes in the incommensurate modulation of the NbO_6 octahedra with temperature and attributed the low-temperature dielectric peak to this effect. Later, Torres-Pardo et al. [64] questioned this relation as the structural characterization by Schefer et al. was not performed in the range of dispersive dielectric maximum, but at higher temperatures. From the structural study of $Sr_2NaNb_5O_{15}$ by transmission electron microscopy, Torres-Pardo et al. [64] showed that the incommensurate phases are neither present nor stabilized with decreasing temperature and the origin of the reentrant relaxor behavior is different. Based on the analysis of the temperature evolution of the lattice strain, they suggested that a subtle rotation of spontaneous polarization towards the *a* axis occurs upon cooling below T_m, which could be associated with "a smeared-out phase transition into a frustrated ferroelectric/ferroelastic low temperature state". The observed relaxor-type dispersion was attributed to the relaxation of PNRs, which coexist with the FE percolation cluster. The decrease in the measured spontaneous polarization on cooling was explained by the increase in the concentration of PNRs, which reduces the volume of the parent FE phase. However, structural evidence for the existence of PNRs was not obtained.

We point out that the above-described anisotropy of tungsten bronze ferroelectric crystals is compatible with the model of transverse freezing known in the physics of magnetic reentrant spin glasses (Figure 23.3). In this model the spontaneous polarization of the FE phase corresponds to the z-component of the order parameter, while the transverse local polarization, which remains dynamic at $T_m < T < T_C$ and freezes at lower temperatures, is considered to be responsible for the permittivity peak at T_m (Figure 23.12(b)) and the remanent polarization observed in the (001) plane below T_m (Figure 23.13). The transverse dipole moment can appear due to the shifts of cations away from the symmetry axis of the tetragonal unit cell. The symmetry prescribes the existence of at least four equivalent positions for the shifted cations, and the thermally activated hopping of the cations among these positions can be responsible for the transverse polarization fluctuations. However, the observed Arrhenius behavior of the characteristic relaxation time suggests that a thermodynamic phase transition to the dipolar glass (or non-ergodic relaxor) phase is absent, and the freezing around T_m is purely kinetic (like in many "normal" dipolar glasses and relaxors). Therefore, the transverse remanent polarization observed at $T < T_m$ is a non-equilibrium quantity. It can be measured by experiment due to a very long relaxation time. Structural verification of this model is yet to be provided.

23.5 Transverse Glassy Freezing and Canonical Relaxors

In the previous section we have considered the examples of materials where the FE phase with the macroscopic polar symmetry exists at temperatures below T_C (as confirmed, for example, by standard X-ray diffraction experiments), and the relaxor behavior appears at lower temperatures. It was noticed [73], however, that even in canonical relaxors where the FE phase is not observed without an external field, some features in the behavior resemble the reentrant rather than "normal" magnetic spin glasses. In particular, the study of the X-ray diffuse scattering in the vicinity of the Bragg peaks in the PMN crystal revealed an unusual behavior of the scattering intensity related to ferroelectric-type fluctuations, which follows a power law $q^{-\alpha}$ at large q with $2 < \alpha < 3$, where q is the deviation of the scattering vector from the reciprocal lattice point. A similar power law dependence was observed in the RSG materials in contrast to the Lorentzian form of scattering found in the materials where the paramagnetic phase transforms directly to the SG phase [17, 23].

The analogy between the reentrant spin glasses and relaxor ferroelectrics is not very surprising, as both are characterized by partially frustrated interactions and both exhibit a mesoscopic or even macroscopic collinear order that exists alongside a glassy order. Subsequent studies based mainly on the analysis of aging phenomena [74–78] provided support to that analogy and suggested that to describe the phase transitions in relaxor ferroelectrics completely, two coexisting order parameters may be needed. In the present section we discuss the results of these investigations.

Aging is a characteristic phenomenon of many disordered materials. The term applies to situations where the properties depend on the time spent by the studied sample under particular conditions. In the context of the present paper we will consider the aging of small-signal AC susceptibility, $\chi = \chi' - i\chi''$ (the dielectric susceptibility and permittivity are related by $\chi = \varepsilon - 1$). One experiment that can conveniently reveal the features of the phenomenon consists in continuous measurements of χ in the course of fast cooling

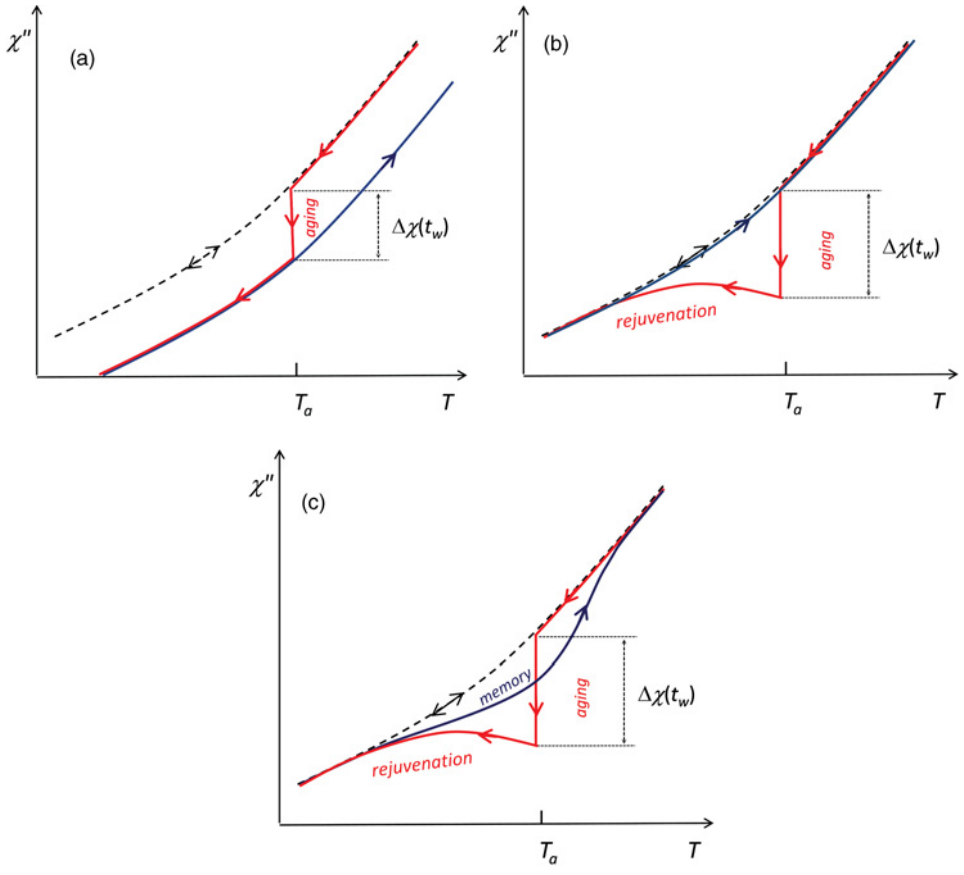

Figure 23.14 *Possible scenarios of aging behavior in ferroic systems: (a) cumulative aging, which can be observed in the FE phase of normal ferroelectrics; (b) aging with rejuvenation, which can be observed in the FM phase of disordered magnets and reentrant spin glasses, and in the FE phase of relaxor ferroelectrics; (c) aging with rejuvenation and memory, which can be observed in the SG phase, RSG phase, and NR phase. In the experiment, the susceptibility is continuously measured while the temperature first decreases, then stabilizes at the aging temperature, T_a, for a waiting time, t_w, then decreases again (red lines), and finally increases (blue line). The dashed line represents the behavior of the same sample if the temperature varies continuously (without aging). For a color version of this figure, see color plate section*

(quenching) of the sample through the phase transition down to a temperature T_a, stabilizing the temperature during some waiting time t_w, further fast cooling down to $T \ll T_a$, and then fast heating up through T_a. The possible variants of the behavior are presented schematically in Figure 23.14 for the most typical case where the susceptibility decreases on cooling and with time. The imaginary part of susceptibility is shown, as it usually reveals more pronounced aging effects than the real part. The drop of χ at T_a (aging) can be quite significant (dozens percent). Qualitative differences can occur in the behavior after aging. The cumulative aging (Figure 23.14(a)) is non-reversible, and the initial (non-aged) value

of χ can be restored only after heating the sample to the high-temperature phase. In other scenarios (Figure 23.14(b) and (c)), cooling after aging results in a comparatively slow variation of χ within a certain temperature interval below T_a, and at low temperatures the value of χ is the same as it would be without aging. This effect of susceptibility restoration is called rejuvenation. However, in some cases the rejuvenated sample still "remembers" that it was previously aged at T_a and upon subsequent warming a significant dip (or "hole") is observed in the $\chi(T)$ dependence around T_a (Figure 23.14(c)). A more detailed description of the aging phenomena in magnetic materials can be found in the review by Vincent [79].

Aging indicates that the system is not in equilibrium and moves slowly to a configuration with lower free energy. In normal ferroelectrics the process is generally related to the peculiarities of the domain structure, which influences the susceptibility significantly. Internal stresses and electric fields can appear in the polydomain sample immediately after the phase transition. Their minimization may occur via rearrangement of domain walls and diffusion of lattice defects [80] and, when an optimal configuration is reached, it is no longer influenced significantly by the temperature variation. As a result, aging appears to be cumulative.

The rejuvenation and memory effects stem from hierarchical organization of the metastable states, which is typical of spin glasses and FM phase in disordered magnets [79, 81]. The characteristic memory holes (Figure 23.14(c)) were observed in the "normal" SG phase or in the RSG phase, and the crossover into the rejuvenation (without memory) regime (Figure 23.14(b)) was found after transformation into the FM phase, which can be obtained by heating from the RSG phase or by increasing the concentration of magnetic atoms in an alloy [81]. An analogous crossover between regimes upon variation of composition or temperature was discovered in relaxor ferroelectrics [82]. In particular, the NR phase of the classical relaxor PMN showed the aging behavior to be very similar to the behavior of the SG or RSG phase, including rejuvenation and memory holes as depicted in Figure 23.14(c) and also the scaling effect, which consists of a special relation between the $\chi''(t_w)$ dependences measured at different frequencies during an isothermal aging. All these dependences can be placed onto a single curve, being plotted as χ'' versus the product $t_w f$. In the $(1-x)$PMN–xPT solid solutions with a large enough x the glassy phase is absent and the phase with a collinear long-range (FE) order was observed. Accordingly, the memory was absent and only rejuvenation was found in the FE phase of the 0.72PMN–0.28PT crystal [75]. In the crystal of 0.9PMN–0.1PT with a lower PT concentration the crossover between the regimes was observed upon temperature variation in the same sample [83], similar to the reentrant spin glasses. Note, however, that the behavior of the relaxors is even more complex, and additional cumulative aging was seen in some temperature intervals. This aging seems to be related to additional microscopic mechanisms not existing in magnetic analogs.

The above-described striking parallels allowed Weissman and co-workers [78] to conclude that not only the relaxation properties, but also the microscopic arrangements of the relaxing entities in relaxor ferroelectrics and in reentrant spin glasses are probably similar in some aspects. They agreed with the common belief that in canonical relaxors like PMN the main contribution to the susceptibly in the vicinity of T_m comes from the thermally activated reorientations of the dipole moments of PNRs. However, in the low-temperature phase where these reorientations are effectively frozen, a different relaxation process becomes important. It was proposed that it is the reorientations of the

polarization components orthogonal to the spontaneous polarization of PNRs that contribute to the dielectric response and glassy aging phenomena observed at $T < T_f$, similar to the transverse (i.e. *xy*) components of magnetization in the RSG phase. According to this picture, the PNRs in relaxors play the role of FM domains in reentrant spin glasses. The difference lies in the fact that in reentrant magnets the longitudinal and transverse components are subject to FM and glassy ordering, respectively, while the behavior of canonical relaxors is more complex: the FE (longitudinal) ordering that occurs inside PNRs is local. The longitudinal polarization component (the polarization of the particular PNR) remains dynamic in a wide temperature range at $T > T_f$ and freezes at T_f alongside the relatively independent transverse component. Therefore, two distinct glassy order parameters exist in parallel.

A number of experimental data support this model, some of which are summarized as follows:

(i) The results of X-ray diffraction [83] and neutron pair distribution function analysis [39] of PMN and 0.9PMN–0.1PT are consistent with the picture in which the symmetry of every perovskite unit cell inside a PNR is monoclinic with the dipole moment directed between <111> and <100>; thus it can be decomposed into the <111> component and the component orthogonal to <111>. All the <111> components inside a particular PNR are ordered along the same <111> direction (which corresponds to the z axis in the model shown in Figure 23.3), while the directions of the orthogonal components remain disordered and may be frozen upon cooling into a transverse spin-glass-like state (like the xy glass in the RSG phase; see Figure 23.3).

(ii) The glassy aging (the magnitude and form of the memory holes) in the 0.92PMN–0.08PT relaxor is practically unaffected by the (field-induced) remanent polarization of the whole sample [76]. This suggests that the reorientations of the longitudinal dipole moments of PNRs, which determine both the remanent polarization of a poled sample and the main part of the small-signal dielectric response, are not related to the observed aging. The glassy aging and the major dialectic response come from the different degrees of freedom.

(iii) The temperature dependence of Barkhausen noise in PMN suggests that the dipoles participating in the glassy freezing possess moments much smaller than the moments of PNRs. These dipoles could be associated with the transverse components of the unit cell moments [78].

(iv) In the uniaxial relaxor $Sr_xBa_{1-x}Nb_2O_6$ where the dipole moments of all PNRs are collinear and no orthogonal component is expected, a spin-glass-like memory is not observed at low temperatures [74].

(v) The isothermal transformation of the NR phase to the FE phase under an external DC field and the transformation of the field-induced FE phase to the ER phase upon heating were found to occur in two steps, separated in time, corresponding to the development of two distinct order parameters related to the longitudinal and transverse polarization components, respectively [77].

Note that the glassy aging, rejuvenation, and memory effects, qualitatively the same as in PMN, were also found in the $(1 - x)$BT–xBS ceramics with $x = 0.3$ [60]. However, the question whether other relaxors follow a similar behavior is still open.

23.6 Reentrant Dipolar Glass State in Quantum Paraelectrics Doped with Dipolar Impurities

Quantum paraelectrics are the incipient ferroelectrics whose FE phonon soft mode tends to condense at a temperature close to 0 K, but quantum fluctuations prevent the condensation and the material remains paraelectric at all temperatures. Dipolar impurities, that is the impurity (doping) ions shifted from the centrosymmetric sites of the paraelectric unit cell, can stabilize the FE phase when their concentration is larger than a critical value, while a lower concentration results in the formation of a dipolar glass state [33, 85]. Some authors qualify these materials as relaxors. From the structural point of view, moderately doped quantum paraelectrics occupy an intermediate position between the dipolar glasses and the canonical relaxor ferroelectrics. The elementary dipole moments associated with the off-center ionic displacements in distinct unit cells are separated by comparatively large distances (like in simple dipolar glasses); however, due to the high (FE soft mode related) polarizability of the lattice a permanently poled dipole is formed around every off-center ion that resembles a PNR [33, 86]. In contrast to the classical relaxors, the formation of polar nanoregions in this case is not a cooperative effect. The observed broad frequency-dependent peak in the temperature dependence of dielectric permittivity is seemingly identical to that detected in canonical relaxors. An example is shown in Figure 23.15, where the relaxor-like permittivity peak is observed at T_m between 45 and 75 K in the perovskite quantum paraelectric $KTaO_3$ doped with Li and Nb. This peak was related to the glassy freezing of the dipole dynamics of the off-centered Li^+ ions that substitute the K^+ ions in their centrosymmetric positions. However, in contrast to canonical relaxors, T_m follows the Arrhenius law (i.e. Equation (23.3) with $T_{VF} = 0$) and the static permittivity follows the Curie–Weiss law in the temperature range, where the frequency-dependent maximum is

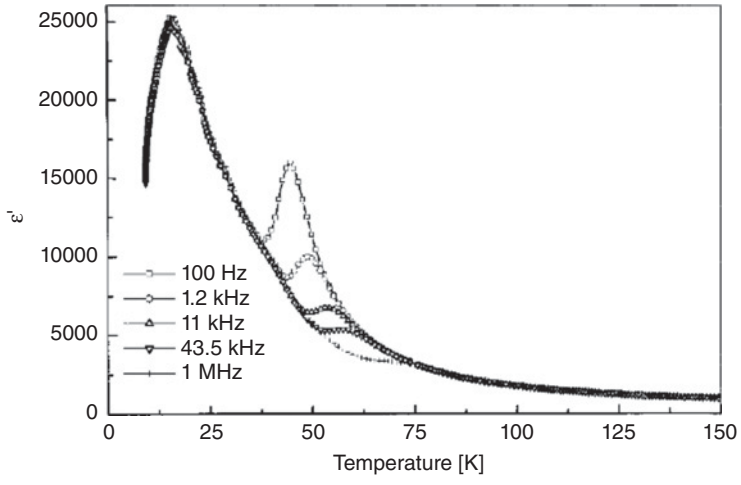

Figure 23.15 *Temperature dependences of the dielectric permittivity in the $K_{0.9986}Li_{0.0014}Ta_{0.976}Nb_{0.024}O_3$ crystal measured at different frequencies. Reprinted (Figure 1) from [87] with permission from Trepakov et al. Copyright (2001), American Physical Society*

observed [87,88]. In the $K_{0.9986}Li_{0.0014}Ta_{0.976}Nb_{0.024}O_3$ crystal presented in Figure 23.15, the dopant concentration is close to the critical value. Thus, besides the formation of the dipolar glass in the Li^+ subsystem, the phonon soft mode-driven FE transition was found at $T_C = 39$ K from Raman scattering and dielectric spectroscopy experiments [87,88]. An additional dielectric peak was observed at 15 K. However, it disappeared in a field-cooled crystal. In contrast to the high-temperature dispersive peak, the low-temperature peak was practically frequency-independent. It was supposed to be associated with the transition into a new glass-like phase. As this phase occurred on cooling from the FE phase, it was qualified as a reentrant dipolar glass-like state. However, later neutron diffraction investigation [89] did not confirm the existence of a normal FE phase. While the lattice parameter passed through a minimum at T_C, no splitting or broadening of the (h00) or (hhh) reflections was found, suggesting that the crystal retained the cubic structure at low temperatures. Nevertheless, the sample was found to be most likely heterogeneous, as comparatively small satellites were observed in the vicinity of the (hhh) reflections below $\sim T_C$, which were related to the clusters of the rhombohedral phase embedded into the cubic matrix.

23.7 Summary and Concluding Remarks

Investigation of the reentrant phases and related phenomena in relaxor ferroelectrics is currently just beginning. It appears to be challenging due to the complexity of the objects to be studied. The results published so far have shown a considerable diversity in the reentrant phenomena in relaxors. An unusual dielectric anomaly, that is a diffuse and dispersive $\varepsilon(T)$ peak located within the temperature range of the FE phase, has been reported in a number of perovskite and tungsten bronze materials. However, in most cases the data are not complete enough to distinguish whether this peak signifies a true thermodynamic phase transition into a glassy phase or results from kinetic Arrhenius-type slowing down of an intrinsic or extrinsic relaxation process. The only reentrant relaxor where the non-Arrhenius relaxation has been verified is the $(1-x)BaTiO_3$–$xBiScO_3$ solid solution system, where the Vogel–Fulcher divergence of the relaxation time has been found, suggesting a "true" glassy freezing of the relaxation dynamics at $0 < T_f < T_C$ (see Section 23.4.1.1). On the contrary, the Arrhenius temperature dependence of the relaxation time has been found for the "transverse" reentrant relaxor-like relaxation in a number of tungsten bronze crystals (see Section 23.4.1.2).

In most of the reported reentrant relaxor cases, the experimental data and suggested models indicate a conservation of the high-temperature FE order at temperatures below the relaxor-type permittivity maximum, that is within the reentrant state. The only result that points to the existence of a "true" reentrant phase, that is a phase less ordered than the high-temperature FE phase, is the decreasing remanent polarization below T_m derived from the FE hysteresis loops in $Sr_2NaNb_5O_{15}$ (Figure 23.11) and some other ceramics. However, in view of the difficulties in the interpretation of the low-temperature FE hysteresis loops, as discussed throughout this review, further investigations of the temperature dependence of spontaneous polarization need to be performed.

The models proposed for the reentrant phenomena in relaxors consider two types of coexistence of the FE order and the glassy subsystem of local dipoles in the reentrant state. The first type implies the presence of the spatial macro- or microscopic heterogeneity where the

material consists of the FE regions and the regions of the less ordered glassy phase. Alternatively, two orthogonal components of the local dipole moment are supposed to exist. One of the components contributes to the collinear order of the FE domains or PNRs. The other component forms a two-dimensional dipole glass in the plane perpendicular to the direction of the collinear order. Further research is needed to clarify the underlying microscopic mechanisms. A great deal of information concerning the reentrant states in relaxors is expected to be generated in the near future, which will be helpful in understanding the relaxor behavior in general.

Acknowledgments

This work was supported by the United States Office of Naval Research (ONR, Grant No. N00014-12-1-1045) and the Natural Science and Engineering Research Council of Canada (NSERC).

References

(1) Tamman, G. (1903) *Kristallisieren und Schmelzen*, Johann Ambrosius Barth, Leipzig.
(2) Rastogi, S., Newman, M., and Keller, A. (1991) Pressure-induced amorphization and disordering on cooling in a crystalline polymer. *Nature*, **353**, 55–57.
(3) Greer, A.L. (2000) Too hot to melt. *Nature*, **404**, 124–135.
(4) Hudson, C.S. (1904) The reciprocative solubility of nicotine in water. *Zeitschrift für Physikalische Chemie*, **47** (1), 113–115.
(5) Narayanan, T. and Kumar, A. (1994) Reentrant phase transitions in multicomponent liquid mixtures. *Physics Reports*, **239**, 135–128.
(6) Lin, T.H., Shao, X.Y., Wu, M.K., et al. (1984) Observation of a reentrant superconducting resistive transition in granular $BaPb_{0.75}Bi_{0.25}O_3$ superconductor. *Physical Review B*, **29** (3), 1493–1496.
(7) Kim, D.C., Kim, J.S., Kang, H.R., et al. (2001) Observation of anomalous reentrant superconductivity in $Sr_{1-x}K_x$ BiO_3. *Physical Review B*, **64**, art. no. 064502.
(8) Heera, V., Fiedler, J., Hubner, R., et al. (2013) Silicon films with gallium-rich nanoinclusions: from superconductor to insulator. *New Journal of Physics*, **15**, art. no. 083022.
(9) Indekeu, J.O. and Berker, A.N. (1988) Molecular structure and reentrant phases in polar liquid crystals. *Journal de Physique France*, **49** (2), 353–362.
(10) Mazza, M.G. and Schoen, M. (2011) Structure and dynamics of reentrant nematics: Any open questions after almost 40 years? *International Journal of Molecular Sciences*, **12** (8), 5352–5372.
(11) Altamirano, N., Kubiznak, D., and Mann, R.B. (2013) Reentrant phase transitions in rotating anti-de Sitter black holes. *Physical Review D*, **88** (10), art. no. 101502(R).
(12) Lines, M.E. and Glass, A.M. (1977) *Principles and Applications of Ferroelectrics and Related Materials*, Clarendon Press, Oxford.
(13) Walker, J.S. and Vause, C.A. (1983) Lattice theory of binary fluid mixtures: phase diagrams with upper and lower critical solution points from a renormalization group calculation. *The Journal of Chemical Physics*, **79** (6), 2661–2676.

(14) Coles, B.R., Sarkissian, B.V.B., and Taylor, R.H. (1978) The role of finite magnetic clusters in Au–Fe alloys near the percolation concentration. *Philosophical Magazine B*, **37** (4), 489–498.
(15) Abdul-Razzaq, W. and Kouvel, J.S. (1984) Spin glassiness and ferromagnetism in disordered Ni–Mn. *Journal of Applied Physics*, **55** (6), 1623–1627.
(16) Maletta, H. (1982) Magnetic ordering in $Eu_xSr_{1-x}S$, a diluted Heisenberg system with competing interactions. *Journal of Applied Physics*, **53** (3), 2185–2190.
(17) Aeppli, G., Shapiro, S.M., Birgeneau, R.J., and Chen, H.S. (1983) Spin correlations and reentrant spin-glass behavior in amorphous Fe–Mn alloys: statics. *Physical Review B*, **28** (9), 5160–5172.
(18) Wong, P.Z., von Molnar, S., Palstra, T.T.M., et al. (1985) Coexistence of spin-glass and antiferromagnetic orders in the Ising system $Fe_{0.55}Mg_{0.45}Cl_2$. *Physical Review Letters*, **55** (19), 2043–2046.
(19) Ryan, D.H. (1992) Exchange frustration and transverse spin freezing, in *Recent Progress in Random Magnets*, edited by R.H. Ryan, World Scientific, Singapore, New Jersey, London, Hong Kong, pp. 1–40.
(20) Mirebeau, I., Hennion, M., Mitsuda, S., and Endoh, Y. (1992) Investigation of the reentrant spin glass phase by neutron scattering, in *Recent Progress in Random Magnets*, edited by R.H. Ryan, World Scientific, Singapore, New Jersey, London, Hong Kong, pp. 41–69.
(21) Sherrington, D. and Kirkpatrick, S. (1975) Solvable models of a spin-glass. *Physical Review Letters*, **35** (26), 1792–1796.
(22) Thomson, J.R., Guo, H., Ryan, D.H., et al. (1992) Magnetic ordering in the three-dimensional frustrated Heisenberg model. *Physical Review B*, **45** (6), 3129–3132.
(23) Aeppli, G., Shapiro, S.M., Maletta, H., et al. (1984) Spin correlations near the ferromagnetic-to-spin-glass crossover. *Journal of Applied Physics*, **55** (6), 1628–1633.
(24) Cowley, R.A., Shirane, G., Birgeneau, R.J., and Svensson, E.C. (1977) Critical scattering near the percolation threshold in $Mn_cZn_{1-c}F_2$. *Physical Review Letters*, **29** (14), 894–897.
(25) Imry, Y. and Ma, S.K. (1975) Random-field instability of the ordered state of continuous symmetry. *Physical Review Letters*, **35** (21), 1399–1401.
(26) Abiko, S., Niidera, S., and Matsubara, F. (2005) Reentrant spin-glass transition in a dilute magnet. *Physical Review Letters*, **94**, art. no. 227202.
(27) Niidera, S. and Matsubara, F. (2007) Fluctuating clusters in a reentrant spin-glass system. *Physical Review B*, **75**, art. no. 144413.
(28) Jonason, K., Mattsson, J., and Nordblad, P. (1996) Dynamic susceptibility of a reentrant ferromagnet. *Physical Review B*, **53** (10), 6507–6513.
(29) Dho, J., Kim, W.S., and Hur, N.H. (2002) Reentrant spin glass behavior in Cr-doped perovskite manganite. *Physical Review Letters*, **89** (2), art. no. 027202.
(30) Kleemann, W., Shvartsman, V.V., Borisov, P., and Kania, A. (2010) Coexistence of antiferromagnetic and spin cluster glass order in the magnetoelectric relaxor multiferroic $PbFe_{0.5}Nb_{0.5}O_3$. *Physical Review Letters*, **105**, art. no. 257202.
(31) Chillal, S., Thede, M., Litterst, F.J., et al. (2013) Microscopic coexistence of antiferromagnetic and spin-glass states. *Physical Review B*, **87**, art. no. 220403.

(32) Ye, Z.G. (1998) Relaxor ferroelectric complex perovskites: structure, properties and phase transitions. *Key Engineering Materials*, 155–156, 81–122.
(33) Samara, G.A. (2003) The relaxational properties of compositionally disordered ABO_3 perovskites. *Journal of Physics: Condensed Matter*, **15** (9), R367–R411.
(34) Bokov, A.A. and Ye, Z.G. (2006) Recent progress in relaxor ferroelectrics with perovskite structure. *Journal of Materials Science*, **41** (1), 31–52.
(35) Burton, B.P., Cockayne, E., Tinte, S., and Waghmare, U.V. (2006) First-principles-based simulations of relaxor ferroelectrics. *Phase Transitions*, **79** (1–2), 91–121.
(36) Cowley, R.A., Gvasaliya, S.N., Lushnikov, S.G., et al. (2011) Relaxing with relaxors: a review of relaxor ferroelectrics. *Advances in Physics*, **60** (2), 229–327.
(37) Shvartsman, V.V. and Lupascu, D.C. (2012) Lead-free relaxor ferroelectrics. *Journal of the American Ceramic Society*, **95** (1), 1–26.
(38) Gehring, P.M. (2012). Neutron diffuse scattering in lead-based relaxor ferroelectrics and its relationship to the ultra-high piezoelectricity. *Journal of Advanced Dielectrics*, **2** (2), art. no. 1241005.
(39) Jeong, I.K., Darling, T.W., Lee, J.K., et al. (2005) Direct observation of the formation of polar nanoregions in $PbMg_{1/3}Nb_{2/3}O_3$ using neutron pair distribution function analysis. *Physical Review Letters*, **94**, art. no. 147602.
(40) Xu, G., Shirane, G., Copley, J.R.D., and Gehring, P.M. (2004) Neutron elastic diffuse scattering study of $Pb(Mg_{1/3}Nb_{2/3})O3$. *Physical Review B*, **69**, art. no. 064112.
(41) Bing, Y.H., Bokov, A.A., and Ye, Z.G. (2011). Diffuse and sharp ferroelectric phase transitions in relaxors. *Current Applied Physics*, **11**, S14–S21.
(42) Hlinka, J. (2012) Do we need the ether of polar nanoregions. *Journal of Advanced Dielectrics*, **2** (2), art. no. 1241006.
(43) Bosak, A., Chernyshov, D., Vakhrushev, S., and Krisch, M. (2012) Diffuse scattering in relaxor ferroelectrics: true three-dimensional mapping, experimental artefacts and modeling. *Acta Crystallographica A*, **68**, 117–123.
(44) Takenaka, H., Grinberg, I., and Rappe, A.M. (2013) Anisotropic local correlations and dynamics in a relaxor ferroelectric. *Physical Review Letters*, **110**, art. no. 147602.
(45) Akbarzadeh, A., Prosandeev, S., Walter, E., et al. (2012) Finite-temperature properties of $Ba(Zr,Ti)O_3$ relaxors from first principles. *Physical Review Letters*, **108**, art. no. 257601.
(46) Hu, W., Hayashi, K., Ohwada, K., et al. (2014) Acute and obtuse rhombohedrons in the local structures of relaxor ferroelectric $Pb(Mg_{1/3}Nb_{2/3})O_3$. *Physical Review B*, **89**, art. no. 140103(R).
(47) Dkhil, B., Gemeiner, P., Al-Barakaty, A., et al. (2009) Intermediate temperature scale T^* in lead-based relaxor systems. *Physical Review B*, **80**, art. no. 064103.
(48) Bokov, A.A., Bing, Y.H., Chen, W., et al. (2003) Empirical scaling of the dielectric permittivity peak in relaxor ferroelectrics. *Physical Review B*, **68**, art. no. 052102.
(49) Bokov, A.A. and Ye, Z.G. (2012) Dielectric relaxation in relaxor ferroelectrics. *Journal of Advanced Dielectrics*, **2** (2), art. no. 1241010.
(50) Jonscher, A.K. (1983) *Dielectric Relaxation in Solids*, Chelsea Dielectrics Press, London.
(51) Tagantsev, A.K. (1994) Vogel–Fulcher relationship for the dielectric permittivity in relaxor ferroelectrics. *Physical Review Letters*, **72** (7), 1100–1103.

(52) Zhao, X., Qu, W., Tan, X., et al. (2007) Electric field-induced phase transitions in (111)-, (110)-, and (100)-oriented $Pb(Mg_{1/3}Nb_{2/3}O_3$ single crystals. *Physical Review B*, **75**, art. no. 104106.
(53) Wang, Y.L., He, Z.B., Damjanovic, D., et al. (2011) Unusual dielectric behavior and domain structure in rhombohedral phase of $BaTiO_3$ single crystals. *Journal of Applied Physics*, **110**, art. no. 014101.
(54) Wang, Y.L., Tagantsev, A.K., Damjanovic, D., and Setter, N. (2007) Giant domain wall contribution to the dielectric susceptibility in $BaTiO_3$ single crystals. *Applied Physics Letters*, **91**, art. no. 062905.
(55) Lei, C. and Ye, Z.G. (2008) Re-entrant-like relaxor behaviour in the new $0.99BaTiO_3$–$0.01AgNbO_3$ solid solution. *Journal of Physics: Condensed Matter*, **20** (23), art. no. 232201.
(56) Lei, C. (2008) *Studies of Novel Lead-Free Piezoelectric and Relaxor Ferroelectric Materials*, PhD Dissertation, Simon Fraser University, Burnaby, BC.
(57) Guo, H.Y., Lei, C., and Ye, Z.G. (2008) Re-entrant type relaxor behavior in $(1 - x)BaTiO_3$–$xBiScO_3$ solid solution. *Applied Physics Letters*, **92**, art. no. 172901.
(58) Guo, H.Y., Lei, C., and Ye, Z.G. (2009) Dielectric and ferroelectric properties of $(1 - x)BaTiO_3$–$xBiScO_3$ solid solution. *Ferroelectrics*, **380**, 63–68.
(59) Datta, K. and Thomas, P.A. (2010) Structural investigation of a novel perovskite-based lead-free ceramics: $xBiScO_3$–$(1 - x)BaTiO_3$. *Journal of Applied Physics*, **107**, art. no. 043516.
(60) Bharadwaja, S.S.N., Kim, J.R., Ogihara, H., et al. (2011) Critical slowing down mechanism and reentrant dipole glass phenomena in $(1 - x)BaTiO_3$–$xBiScO_3$ ($0.1 \leq x \leq 0.4$): the high energy density dielectrics. *Physical Review B,* **83**, art. no. 024106.
(61) Simon, A., Ravez, J., and Maglione, M. (2005) Relaxor properties of $Ba_{0.9}Bi_{0.067}(Ti_{1-x}Zr_x)O_3$ ceramics. *Solid State Sciences*, **7** (8), 925–930.
(62) Castel, E., Josse, M., Michau, D., and Maglione, M. (2009) Flexible relaxor materials: $Ba_2Pr_xNd_{1-x}FeNb_4O_{15}$ tetragonal tungsten bronze solid solution. *Journal of Physics: Condensed Matter*, **21**, art. no. 452201.
(63) Kleemann, W. (2012) Random fields in relaxor ferroelectrics – a jubilee review. *Journal of Advanced Dielectrics*, **2** (2), art. no. 1241001.
(64) Torres-Pardo, A., Jimenez, R., Gonzalez-Calbet, J.M., and Garcıa-Gonzalez, E. (2011). Structural effects behind the low temperature nonconventional relaxor behavior of the $Sr_2NaNb_5O_{15}$ bronze. *Inorganic Chemistry*, **50** (23), 12091−12098.
(65) Kinka, M., Josse, M., Castel, E., et al. (2012) Coexistence of ferroelectric and relaxor states in $Ba_2Pr_xNd_{1-x}FeNb_4O_{15}$ ceramics. *IEEE Transactions on Ultrasonics, Ferroelectrics, and Frequency Control*, **59** (9), 1879–1882.
(66) Garcıa-Gonzalez, E., Torres-Pardo, A., Jimenez, R., and Gonzalez-Calbet, J.M. (2007) Structural singularities in ferroelectric $Sr_2NaNb_5O_{15}$. *Chemistry of Materials*, **19** (14), 3575–3580.
(67) Li, K., Zhu, X.L., Liu, X.Q., and Chen, X.M. (2013) Re-entrant relaxor behavior of $Ba_5RTi_3Nb_7O_{30}$ (R = La, Nd, Sm) tungsten bronze ceramics. *Applied Physics Letters*, **102**, art. no. 112912.
(68) Ko, J.H., Kojima, S., Lushnikov, S.G., et al. (2002) Low-temperature transverse dielectric and pyroelectric anomalies of uniaxial tungsten bronze crystals. *Journal of Applied Physics*, **92** (3), 1536–1543.

(69) Buixaderas, E., Savinov, M., Kempa, M., et al. (2005) Infrared and dielectric spectroscopy of the relaxor ferroelectric $Sr_{0.61}Ba_{0.39}Nb_2O_6$. *Journal of Physics: Condensed Matter*, **17** (4), 653–666.
(70) Xu, Y., Li, Z., Li, W., and Wang, H. (1989) Phase transition of some ferroelectric niobate crystals with tungsten-bronze structure at low temperatures. *Physical Review B*, **40** (17), 11902–11908.
(71) Schefer, J., Schaniel, D., Pomjakushin, V., et al. (2006) Structural properties of $Sr_{0.61}Ba_{0.39}Nb_2O_6$ in the temperature range 10–500 K investigated by high-resolution neutron powder diffraction and specific heat measurements. *Physical Review B*, **74** (13), art. no. 134103.
(72) Stephanovich, V.A. (2010) Tetragonal tungsten bronze compounds: relaxor versus mixed ferroelectric–dipole glass behavior. *Journal of Physics: Condensed Matter*, **22** (23), art. no. 235902.
(73) Vakhrushev, S., Nabereznov, A., Sinha, S.K., et al. (1996) Synchrotron X-ray scattering study of lead magnoniobate relaxor ferroelectric crystals. *Journal of Physics and Chemistry of Solids*, **57** (10), 1517–1523.
(74) Chao, L.K., Colla, E.V., Weissman, M.B., and Viehland, D.D. (2005) Aging and slow dynamics in $Sr_xBa_{1-x}Nb_2O_6$. *Physical Review B*, **72**, art. no. 134105.
(75) Colla, E.V., Chao, L.K., and Weissman, M.B. (2001) Multiple aging mechanisms in relaxor ferroelectrics. *Physical Review B*, **63**, art. no. 134107.
(76) Colla, E.V., Griffin, P., Delgado, M., and Weissman, M.B. (2008) Polarization-independent aging in the relaxor $0.92PbMg_{1/3}Nb_{2/3}O_3$–$0.08PbTiO_3$. *Physical Review B*, **78**, art. no. 064103.
(77) Colla, E.V. and Weissman, M.B. (2005) Two-step phase changes in cubic relaxor ferroelectrics. *Physical Review B*, **72**, art. no. 104106.
(78) Weissman, M.B., Colla, E.V., and Chao, L.K. (2003) Noise and aging of relaxor ferroelectrics. In *Fundamental Physics of Ferroelectrics 2003 – AIP Conference Proceedings No. 677*, edited by R. Davies and D.J. Singh, AIP, Williamsburg, pp. 33–40.
(79) Vincent, E. (2007) Ageing, rejuvenation and memory: the example of spin-glasses. In *Ageing and the Glass Transition, Lecture Notes Physics 716*, edited by M. Henkel, M. Pleimling, and R. Sanctuary, Springer, Berlin Heidelberg, pp. 7–60.
(80) Damjanovic, D. (1998) Ferroelectric, dielectric and piezoelectric properties of ferroelectric thin films and ceramics. *Reports on Progress in Physics*, **61**, 1267–1324.
(81) Vincent, E., Dupuis, V., Alba, M., et al. (2000) Aging phenomena in spin-glass and ferromagnetic phases: domain growth and wall dynamics. *Europhysics Letters*, **50** (i), 674–680.
(82) Colla, E.V., Chao, L.K., Weissman, M.B., and Viehland, D.D. (2000) Aging in a relaxor ferroelectric: scaling and memory effects. *Physical Review Letters*, **85**, 3033–3036.
(83) Dkhil, B., Kiat, J.M., Calvarin, G., et al. (2001) Local and long range polar order in the relaxor–ferroelectric compounds $PbMg_{1/3}Nb_{2/3}O_3$ and $PbMg_{0.3}Nb_{0.6}Ti_{0.1}O_3$. *Physical Review B*, **65**, art. no. 024104.
(84) Chao, L.K., Colla, E.V., and Weissman, M.B. (2006). Aging in the relaxor ferroelectric $(PbMn_{1/3}Nb_{2/3}O_3)_{0.90}$ $(PbTiO_3)_{0.10}$. *Physical Review B*, **74**, art. no. 014105.
(85) Hochli, U.T., Knoor, K., and Loidl, A. (1990) Orientational glasses. *Advances in Physics*, **39** (5), 405–615.

(86) Toulouse, J. and Pattnaik, R.K. (1996) Pretransitional condensation in mixed ferroelectrics. *Journal of Physics and Chemistry of Solids*, **57**, 1473–1477.
(87) Trepakov, V.A., Savinov, M.E., Giulotto, E., et al. (2001) Dipole ordering effects and reentrant dipolar glass state in $KTaO_3$:Li,Nb. *Physical Review B*, **63**, art. no. 172203.
(88) Trepakov, V., Galinetto, P., Giulotto, E., et al. (2002) Recent developments in $K_{1-x}Li_xTa_{1-y}Nb_yO_3$ investigations. *Ferroelectrics*, **267**, 221–228.
(89) Borisov, S.A., Vakhrushev, S.B., Koroleva, E.Y.U., et al. (2007) Investigation into the evolution of the structure of $K_{1-x}Li_xTa_{1-y}Nb_yO_3$ single crystals under variations in temperature. *Crystallography Reports*, **52** (3), 440–446.